The role of *Cilk1* in tooth pattern formation via Hedgehog pathway

Minjae Kyeong

The graduate School

Yonsei University

Department of Applied Life Science

The role of *Cilk1* in tooth pattern formation via Hedgehog pathway

Directed by Professor Sung-Won Cho

A Dissertation Thesis

Submitted to the Department of Applied Life Science

and the Graduate School of Yonsei University

in partial fulfilment of the requirements

for the degree of Doctoral Philosophy

Minjae Kyeong

June 2024

This certifies that the doctoral dissertation

of Minjae Kyeong is approved.

Thesis Supervisor: Prof. Sung-Won Cho

Thesis Committee Member: Prof. Seok-Jun Moon

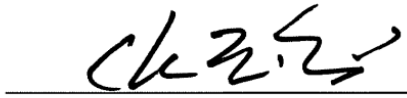

Thesis Committee Member: Prof. Eui-Sic Cho

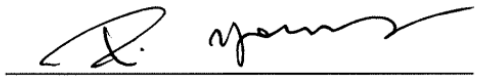

Thesis Committee Member: Prof. Young-Bum Park

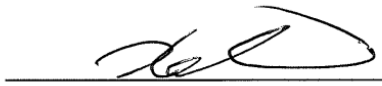

Thesis Committee Member: Prof. Hyuk-Wan Ko

The graduate School
Yonsei University
June 2024

Acknowledgement

본 학위논문을 완성하기까지 수많은 분들의 아낌없는 조언과 도움이 있었습니다. 학위 과정 동안 부족한 저를 이끌어주시고 진정한 연구자의 길로 인도해주신 조성원 교수님께 깊은 감사와 존경을 표합니다. 바쁘신 와중에도 논문 심사를 맡아주시고 귀중한 조언을 해주신 문석준 교수님, 조의식 교수님, 박영범 교수님, 고혁완 교수님께도 진심으로 감사드립니다. 학위 심사에서 받은 교수님들의 조언과 질문을 곰곰이 되새기며, 논문의 핵심 주제와 논의 사항을 더욱 깊이 있게 다듬을 수 있었습니다. 심사에 참여해주신 모든 교수님께 진심으로 감사드립니다.

대학원 생활을 함께하며 힘이 되어준 Dinuka Adasooriya 선생님, Kan Shiqi 선생님 감사를 드립니다. 함께 조교 생활을 하며 용기를 북돋아준 김지우 선생님께도 감사드립니다. 긍정적인 에너지로 힘든 시간을 이겨낼 수 있게 해준 구강생물학교실 선생님들께 감사의 마음을 전합니다.

더불어, 긴 시간 동안 묵묵히 저를 지지해준 모든 친구들에게도 깊은 감사를 드립니다. 마지막으로, 늘 곁에서 항상 버팀목이 되어주고 응원과 격려를 보내주신 부모님과 동생에게 사랑과 감사의 마음을 전합니다.

2024년 6월

저자 씀

TABLE OF CONTENTS

LIST OF FIGURES

LIST OF TABLES

ABSTRACT

The role of *Cilk1* in tooth pattern formation via Hedgehog pathway

Minjae Kyeong

Department of Applied Life Science

The Graduate School, Yonsei University

(Directed by Professor Sung-Won Cho)

Primary cilium is a solitary organelle that transmits chemical and mechanical stimuli to the cell during development and tissue homeostasis. *Cilk1* (Ciliogenesis

associated kinase 1), which is a highly conserved serine/threonine-protein kinase, localizes in primary cilia and regulates formation and function of primary cilia. It has been reported that the loss of *Cilk1* disrupts the regulation of ciliary transport and Hedgehog signaling during development, and leads to severe ciliopathy phenotypes such as polydactyly, edema, cleft palate with perinatal lethality. However, tooth phenotype in *Cilk1*-deficient mice has not been reported yet. In the present study, *Cilk1*-deficient mice showed supernumerary teeth developing in both the maxilla and mandible, where they showed elongated cilia length. Tooth pattern was altered in *Cilk1*-deficient mice due to reduced Hedgehog signaling activity. The correlation of tooth patterns along the Hedgehog pathway was confirmed by cross mating with PCS1−MRCS1$^{\triangle/\triangle}$ mice, which is a *Shh* enhancer deleted mice that exhibit supernumerary teeth. In *Cilk1*$^{-/-}$;PCS1−MRCS1$^{\triangle/\triangle}$ mice, supernumerary tooth enlargement and molar fusion were observed. Taken together, *Cilk1* regulates the tooth patterning by modulating the Hedgehog signaling activity in developing mice.

Keywords: *Cilk1*, Primary cilia, Hedgehog signaling, Tooth development, Supernumerary teeth, Molar fusion

I. Introduction

Primary cilia are microtubule-based organelles projecting from the surface of most mammalian cells. Primary cilia can sense chemical and mechanical signals from the extracellular environment and transduce these signals into the intracellular signaling to regulate fundamental cellular functions during development and homeostasis (Christensen et al. 2007).

Morphological abnormalities or dysfunction of primary cilia lead to ciliopathies, which are a group of syndromes impacting nearly all organs of the body, resulting from dysfunction in sensory and signaling activities (Reiter and Leroux 2017). Furthermore, there are more than 200 putative and more than 150 known ciliopathy-related genes, including *Ift88*, *Evc*, *Evc2*, *Ofd1* and *Cilk1* (Mill, Christensen, and Pedersen 2023; Anvarian et al. 2019; Yanardag and Pugacheva 2021).

Cilk1 (Ciliogenesis associated kinase 1), which was previously known as *Ick* (intestinal cell kinase) gene, is a highly conserved serine/threonine protein kinase that is extensively distributed in development (Fu et al. 2019). Protein kinases represent one of the largest and most functionally diverse gene families in eukaryotes (Manning et al. 2002). Through phosphorylation, kinases can regulate the activity, localization, and overall function of numerous target proteins. They are essential for signal transduction and the coordination of complex cellular processes. Notably, cyclin-dependent kinases (CDKs) and

mitogen-activated protein (MAP) kinases are critical in regulating mammalian cell proliferation and division (Lew 2003; Durandau and Pelet 2021).

Cilk1 is one of the key regulators of the turnaround process in primary cilia and binds to the IFT-B complex and is transported via binding to the IFT-B complex, causing it to localize at the ciliary tips (Nakamura et al. 2020; Satoda et al. 2022a; Satoda et al. 2022b). Moreover, *Cilk1* loss of function results in elongated cilia and decreased Hedgehog signaling (Yang, Roine, and Makela 2013; Nakamura et al. 2020).

Human CILK1 gene mutations result in ciliopathies like endocrine-cerebro-osteodysplasia (ECO) syndrome. Numerous phenotypic abnormalities, including cleft palate, hydrocephalus, and polydactyly are shown in *Cilk1*$^{-/-}$ mice and are associated with the human ECO syndrome (Moon et al. 2014; Oud et al. 2016; Lahiry et al. 2009).

Tooth represents an excellent organ for the study of developmental dynamics and morphogenesis (Salazar-Ciudad 2012). Teeth are ectodermal organs that originate from the cross-talk between dental mesenchyme and dental epithelium (Thesleff 1995; Abigail S. Tucker 1998; Thesleff 2003). The tooth morphogenesis begins with thickening of the dental epithelium and progresses through the lamina, bud, cap, and bell stage. After tooth morphogenesis, cell differentiation, hard tissue formation in crown and root, and the eruption occur subsequently. For the precise temporospatial tooth development, the epithelial mesenchymal interactions are essential (Jernvall and Thesleff 2000).

Primary cilia are present in the dental epithelium and mesenchyme at the early

stages of tooth development, and subsequently during the differentiation of cells and the production of hard tissues. Primary cilia are cellular antennae for biochemical signals during interactions between both dental epithelium and mesenchyme (Hampl et al. 2017).

Primary cilia are involved in signal transduction of several signaling pathways, such as Hedgehog (Goetz and Anderson 2010), Wnt, fibroblast growth factor (FGF), Hippo, mTor, Notch, and platelet-derived growth factor (PDGF) (Wheway, Nazlamova, and Hancock 2018; Lee 2020). Among these pathways, it has been reported that primary cilia are most closely involved in the Hedgehog pathway (Lee 2020). Ciliary Hedgehog signaling has been also reported in tooth development (Thivichon-Prince et al. 2009; Ohazama et al. 2009; Nakatomi et al. 2013; Liu et al. 2014; Zhang et al. 2022). Hedgehog signaling is essential for pattern formation of many organs including teeth. It has been reported that supernumerary teeth or molar fusion were induced in several mutant mice depending on the level of Hedgehog signaling activity. The deletion of MRCS1 and PCS1, two oral-specific cis-regulatory element enhancers of Sonic hedgehog (*Shh*), induced the formation of supernumerary teeth both in maxilla and mandible in mice (Seo et al. 2018), while molar fusion was reported in *Krt14-cre;Shh*$^{flox/flox}$ mice and *Krt14-cre;Smo*$^{flox/flox}$ mice. Consistently, previous studies proposed that primary cilia play a pivotal role in tooth pattern formation. Many mutant mice which lacks of primary cilia-related genes, such as *Evc1, Evc2, Fuz, Ift88, Ift121, Ift122, Kif3a,* and *Ofd1*, demonstrated abnormal craniofacial defects and tooth patterns. The deletion of *EVC2, IFT121/122, OFD1 or CILK1* is associated with abnormal tooth formation such as supernumerary tooth, hypodontia,

oligodontia, dysplastic teeth, natal teeth in humans (Baujat and Le Merrer 2007; Oud et al. 2016; Walczak-Sztulpa et al. 2010; Levin et al. 1977; Dodge and Kernohan 1967). On the other hand, in mouse models, the deletion of *Ofd1* or *Ift88* results in the formation of supernumerary teeth (Thivichon-Prince et al. 2009; Ohazama et al. 2009), and deletion of *Evc* and *Evc2* leads to molar fusion (Nakatomi et al. 2013; Hampl et al. 2017). However, the deletion of cilia-related genes such as *Ift88*, *Ofd1*, and *Kif3a* is highly lethal to embryonic growth and development, often resulting in embryonic lethality before tooth patterning formation (Willaredt et al. 2008; García-García et al. 2005; Ferrante et al. 2006). Due to these challenges, research on tooth patterning has shifted from using null alleles of these genes to utilizing hypomorphic allele mutations or the Cre-loxP system. While *Cilk1* also exhibits embryonic lethality, it dies after tooth patterning is complete, making *Cilk1* knockout mice suitable for studying tooth patterning by modulating Hedgehog pathway activity. However, the tooth pattern of *Cilk1*$^{-/-}$ mice has not yet been reported.

In the present study, in order to better understand the role of Cilk1 in tooth patterning, gene expression pattern of *Cilk1* was investigated by the using RNA in situ hybridization and single-cell RNA sequencing analysis. The role of *Cilk1* in tooth development was explored by examining changes in tooth patterns of molars in *Cilk1*-deficient mice. The relationship between primary cilia and Hedgehog signaling activity was examined in *Cilk1*-deficient mice. Furthermore, through the analysis of various intricate tooth patterns governed by ciliary Hedgehog signaling, a theoretical mechanism for understanding tooth patterning was suggested.

II. Materials and Methods

1. Single-cell RNA sequencing analysis

Publicly available single-cell RNA sequencing (scRNA-seq) datasets of E14.5 and E16.5 mouse molars were obtained from the Gene Expression Omnibus (GEO) under accession number GSE189381 (Jing et al. 2022). These pre-processed count matrices were imported into the Cellenics® community instance (https://scp.biomage.net/) hosted by Biomage (https://biomage.net/) for further analysis and visualization. Cell barcodes were filtered sequentially using the platform's automatic settings, including cell size distribution, mitochondrial content, number of genes vs UMI, and doublet filters. Post-filtering, 30,744 cells from E14.5 and 29,307 cells from E16.5 datasets were retained for analysis. The two E14.5 datasets and the E16.5 dataset were integrated separately using the "Harmony" method and normalized with the "LogNormalize" function. The top 2000 highly variable genes (HVGs) were selected using the variance stabilizing transformation (VST) technique. Dimensionality reduction was performed using principal component analysis (PCA) with 30 principal components (PCs) for both E14.5 and E16.5 datasets, explaining over 90% of the total variance. Cell clusters were generated with the Louvain method and visualized using Uniform Manifold Approximation and Projection (UMAP) embedding at a resolution of 0.3. All cell clusters were manually annotated based on existing literature (Jing et al. 2022).

2. Animals

All animal experiments were performed under approved protocols of the Intramural Animal Use and Care Committee of the Yonsei University College of Dentistry. All mice were used for the study after euthanization utilizing CO_2 exposure at selected postnatal ages and embryonic days. A mix of males and females was assigned without considering the sex, and at least one individual from each sex was included in each group after screening for the genotype with PCR. The *Cilk1* KO mutant, which was a kind gift from Professor H.W. Ko (Moon et al. 2014) is maintained in the C57BL/6 background. PCS1−MRCS1$^{\triangle/\triangle}$ mice with a deletion of a 70 kb region from PCS1 to MRCS1 were previously described (Seo et al. 2018). All *Cilk1*$^{-/-}$ mice and *Cilk1*$^{-/-}$;PCS1−MRCS1$^{\triangle/\triangle}$ mice display perinatal lethality.

3. Whole mount in situ hybridization

Maxillae and mandibles were dissected mouse embryos and fixed overnight in 4% paraformaldehyde (PFA) in DEPC-PBS, washed with DEPC-PBS, dehydrated in graded methanol, and permeabilized by proteinase K. Specimens were then hybridized with digoxigenin-labelled antisense RNA probes followed by incubation in anti-Dig antibody conjugated with alkaline phosphatase. Colorimetric reaction was carried out using 4-nitro-blue-tetrazolium (NBT) and 5-bromo-4chloro-3-indolyl-phosphate (BCIP) as the substrate.

4. Section in situ hybridization

Mandibles were dissected wild-type mouse embryos at E13.5, E14.5, E15.5 and E16.5 on cold DEPC-PBS and fixed with 4% PFA in DEPC-PBS overnight at 4°C with rocking. After being rinsed in DEPC-PBS, the samples were decalcified for 3 hours at 4°C using 10% EDTA in DEPC-PBS. Decalcified samples were washed with DEPC-PBS followed by a saline wash. Samples were dehydrated with a graded ethanol series. Embryo samples were embedded in paraffin and sectioned at 5 μm thickness. Advanced Cell Diagnostics (Newark, USA) designed and manufactured antisense *Cilk1* RNA probes. The RNAscope® 2.5 High Definition (HD) assay-brown (Advanced Cell Diagnostics) was used for in situ hybridization in accordance with the manufacturer's instructions for 322452 (FFPE sample preparation and pretreatment) and 322310 (RNAscope® 2.5 HD Detection Reagent-brown). Mm-Cilk1 (1177181, targeting NM_001163780.1, nucleotide 1358-2353) RNA probe was used.

5. Three-dimensional (3D) reconstruction using computed tomography.

The dissected embryo heads were stained with phosphotungstic acid hydrate (P4006-10G, Sigma-Aldrich) and scanned by a micro-computed tomography (CT) system (Skyscan 1173; Bruker, Kontich, Belgium) using 90 kV, 88 μA, 360° rotation with a step of 0.3°, pixel size of 6 μm and an aluminum filter (1.0 mm of thickness) and reconstructed by the NRecon software (Bruker). The reconstructions were visualized and converted to

3D volumes using the software 3D slicer (Fedorov et al. 2012).

6. Length measurement in molar, incisor, snout and mandible

Tooth size and bone length were measured on the micro-CT sections. The mesiodistal length was measured for molar size. The size of incisor was measured from the incisal tip to the cervical loop. Since the geometric morphometric analysis is difficult to apply to the developing mouse skull at PN 0, the anteroposterior length of maxilla and mandible bones harboring molars and incisors was measured. For maxilla, the snout length was measured from distance from the interpupillary axis to the labial alveolar bone was measured as described previously (Kanady et al. 2015). For mandible, the distance from the posterior end of the condyle to the labial surface of alveolar bone was measured as usual.

7. RNA sequencing analysis

To measure relative amount of *Cilk1* gene expression in tooth germ, maxilla tooth germ was dissected at cap stage in DEPC-PBS. The 0.5 mm zirconia beads were used to homogenize tooth germ samples in TRIZOL ® (Invitrogen) using the Bullet Blender ® homogenizer (Next Advance, USA). Chloroform was used to phase separate the total RNA, and isopropyl alcohol was used to precipitate it. After being cleaned with 75% ethanol, the RNA pellet was eluted using RNase free water. NanoDrop (Thermo Fisher Scientific, USA)

was used to measure the concentration and quality of RNA. Paired-end reads were produced after the library was built and sequenced on an Illumina platform. following the mapping of the quality control reads into the reference genome (mm10). Using featureCounts v1.5.0-p3, the read counts mapped to each gene were calculated and the FPKM of every gene was computed by taking into account the gene's length and the read counts mapped to it.

The number of reads mapped to each gene was quantified using featureCounts v1.5.0-p3, and FPKM values were calculated based on gene length and read counts. Differential expression analysis between the two conditions was performed using the edgeR R package (3.22.5), with read counts adjusted by a scaling normalization factor. P-values were adjusted using the Benjamini & Hochberg method, and a corrected Padj value of 0.05 and an absolute fold change of 1.5 were set as the threshold for significance. Gene Ontology (GO) enrichment analysis of differentially expressed genes were carried out using ShinyGo 0.77 (http://bioinformatics.sdstate.edu/go/). GO terms with corrected P-values below 0.05 were considered significantly enriched.

8. Measurement of the length and frequency of primary cilia.

For measurement of the length of primary cilia body, immunofluorescent were performed and stained with Arl13b (CL488-17711, Proteintech). Confocal microscope the Zeiss LSM 900 (Carl Zeiss, Jena, Germany) was used to capture the images. DAPI-positive

nuclei and Arl13b-positive primary cilia were counted. The Zeiss Zen 3.3 (blue edition) program (Carl Zeiss) was used to measure the length of the cilia bodies in each mutant mouse. The entire length of the primary cilia was captured on a single plane (7 μm thickness) using confocal microscopy Z-stack images (DAPI, Cell Biolabs)

9. Statistical analysis

One-way analysis of variance (ANOVA) with Tukey's test multiple comparisons for the M1/M2 ratio and Student's t-tests (two-tailed) for ciliary length and mice incisor length were used for statistical comparisons. Every graph was visualized with Prism 8.0 (GraphPad, San Diego, CA, USA). P value less than 0.05 was considered a statistically significant difference. * and ** indicate $p < 0.05$ and $^{**}p < 0.01$, respectively. P value larger than 0.05 was considered a statistically non-significant difference (NS).

III. Results

1. *Cilk1* was expressed in both the dental epithelium and mesenchyme in developing teeth

To explore when and where *Cilk1* is expressed during tooth development, recently published single-cell RNA sequencing data were utilized to analyze cell clustering in mouse molars at E14.5 and E16.5 (Jing et al. 2022).

The UMAP visualization illustrated the unbiased detection of 11 clusters at E14.5 and 14 clusters at E16.5 in molars. *Cilk1* was expressed across both the epithelium and mesenchyme during developmental stages (Fig. 1B, J). Other primary cilia-related genes also were expressed throughout the epithelium and mesenchyme (Fig. 1C−H, K−P). In frontal sections of the mandibular first molar (M1) (Fig. 2A−D), cells expressing *Cilk1* were generally located in both the epithelium and mesenchyme from E13 to E16. The expression of *Cilk1* in most cells in tooth germs and their surrounding tissues suggests that *Cilk1* potential involvement in the function or formation of primary cilia during tooth development.

2. *Cilk1* deletion led to the development of supernumerary tooth.

Morphological abnormalities were observed in *Cilk1*$^{-/-}$ mice from E12 to E18 (Fig. 3). *Cilk1*$^{-/-}$ mice exhibited cleft palate (Fig. 3B) and lobulated tongue (Fig. 3D, F, H), which are consistent with the results of previous report (Moon et al. 2014). Cleft palate

and lobulated tongue were observed with 100% probability in *Cilk1*$^{-/-}$mice.

Meanwhile, in tooth development, *Cilk1*$^{-/-}$mice showed the supernumerary teeth (R2) at E14.5 and E16.5 (Fig. 3L, P). At E14.5, one molar was observed in each of wild-type and *Cilk1*$^{-/-}$mice, and the molar in the wild-type mice was larger than that of *Cilk1*$^{-/-}$mice. At E16.5, two molars were observed. While the mesial molar was larger than the distal molar in the wild-type, the mesial molar was smaller than the distal molar in *Cilk1*$^{-/-}$mice. This abnormal phenotype represents a typical tooth pattern of mouse dentition which have supernumerary tooth (Ohazama et al. 2009). Based on this patterning, the tooth germ formed at E14.5 can be regarded as supernumerary tooth. Supernumerary tooth was observed in 100% of the maxilla and mandible in *Cilk1*$^{-/-}$mice.

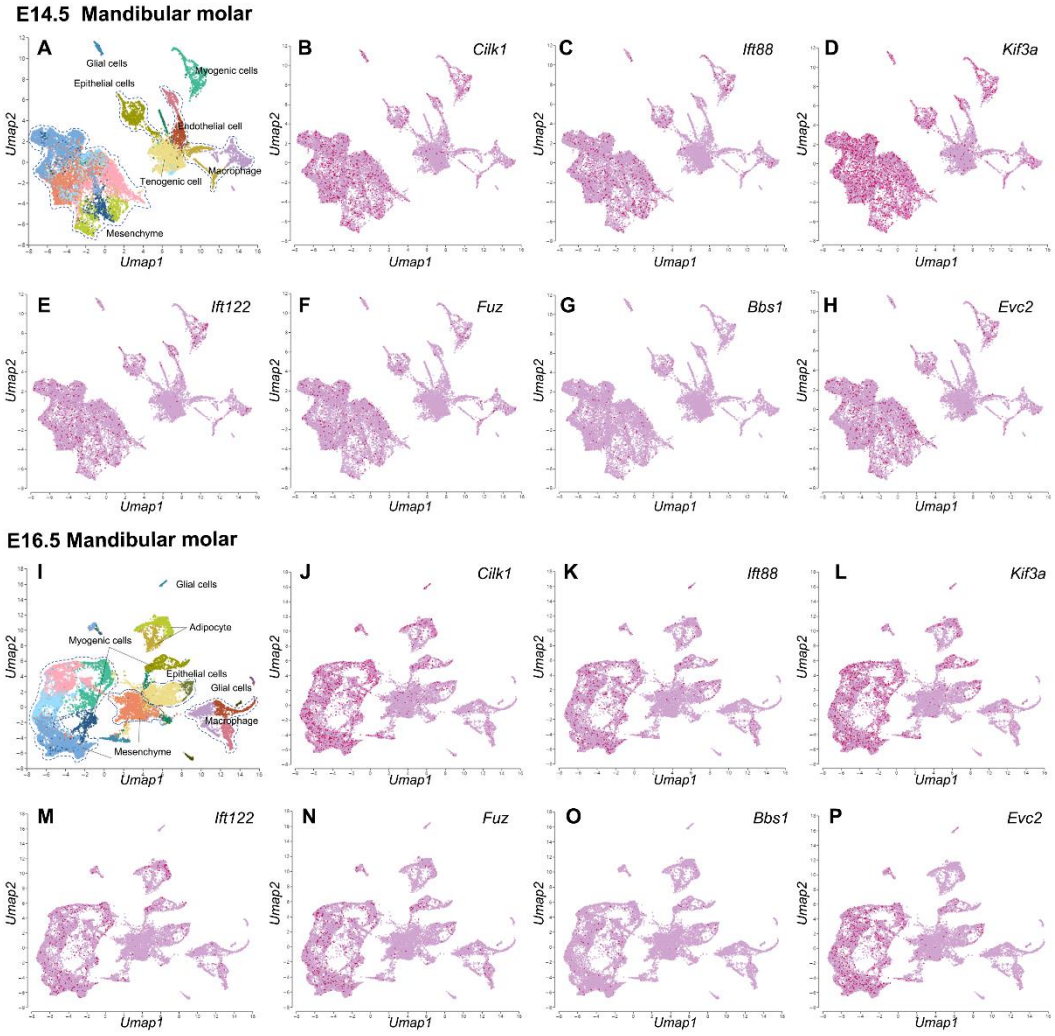

Figure 1. Expression patterns of primary cilia-associated genes in multiple cell types detected from single-cell RNA sequencing data of mouse molar tooth germs at E14.5 and E16.5.

(A, I) Annotated single-cell transcriptomic map of mouse molars at E14.5 (A) and E16.5 (I) from data generated using scRNA-seq applied from Jing, J. et al.

(B, J) Expression profiles of *Cilk1* among defined cell clusters shown in UMAP. (C−H, K−P) Expression of genes related to primary cilia at each developmental stage. (B, J) *Cilk1*, (C, K) *Ift88*, (D, L) *Kif3a*, (E, M) *Ift122*, (F, N) *Fuz*, (G.O) *Evc*, (H, P) *Evc2*.

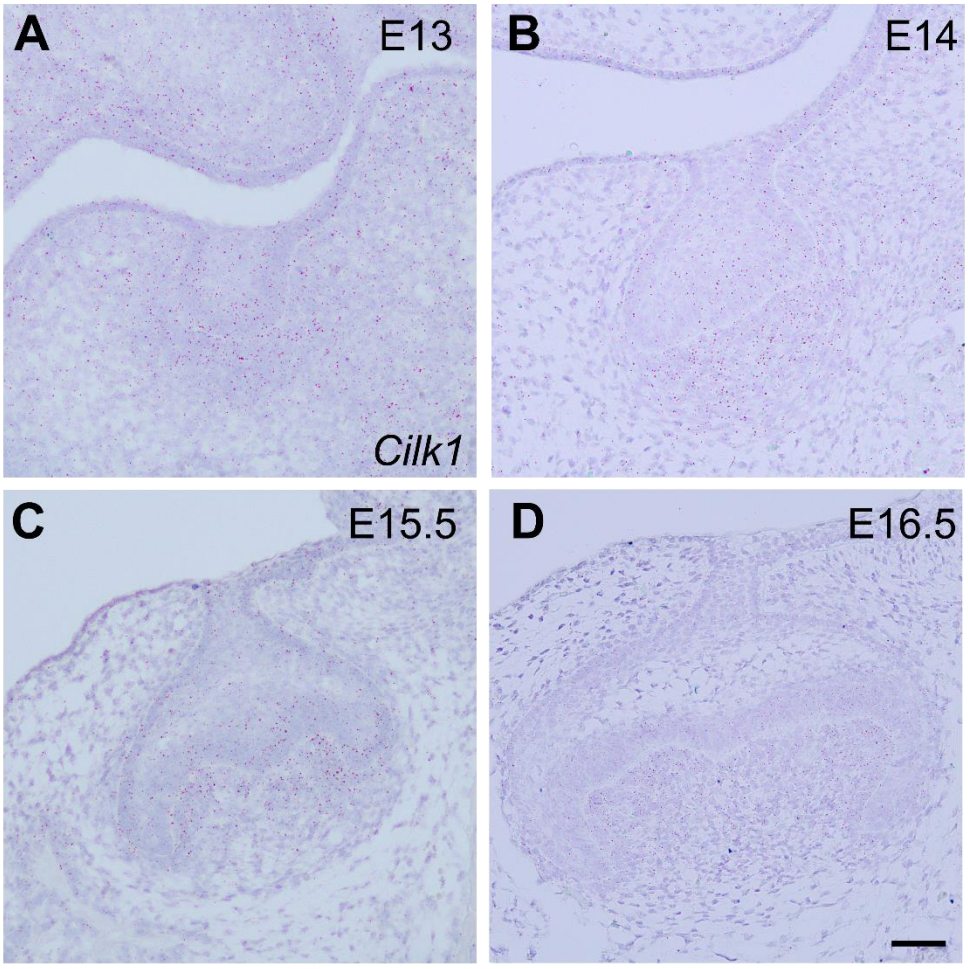

Figure 2. Expression pattern of *Cilk1* during mouse tooth development

The *Cilk1* expression (small brown dots) in frontal sections of the developing first molars (M1) of wild-type mice at E13, E14, E15.5 and E16.5. *Cilk1* is weakly expressed in dental epithelium and dental mesenchyme. Scale bar: A−D, 50 μm.

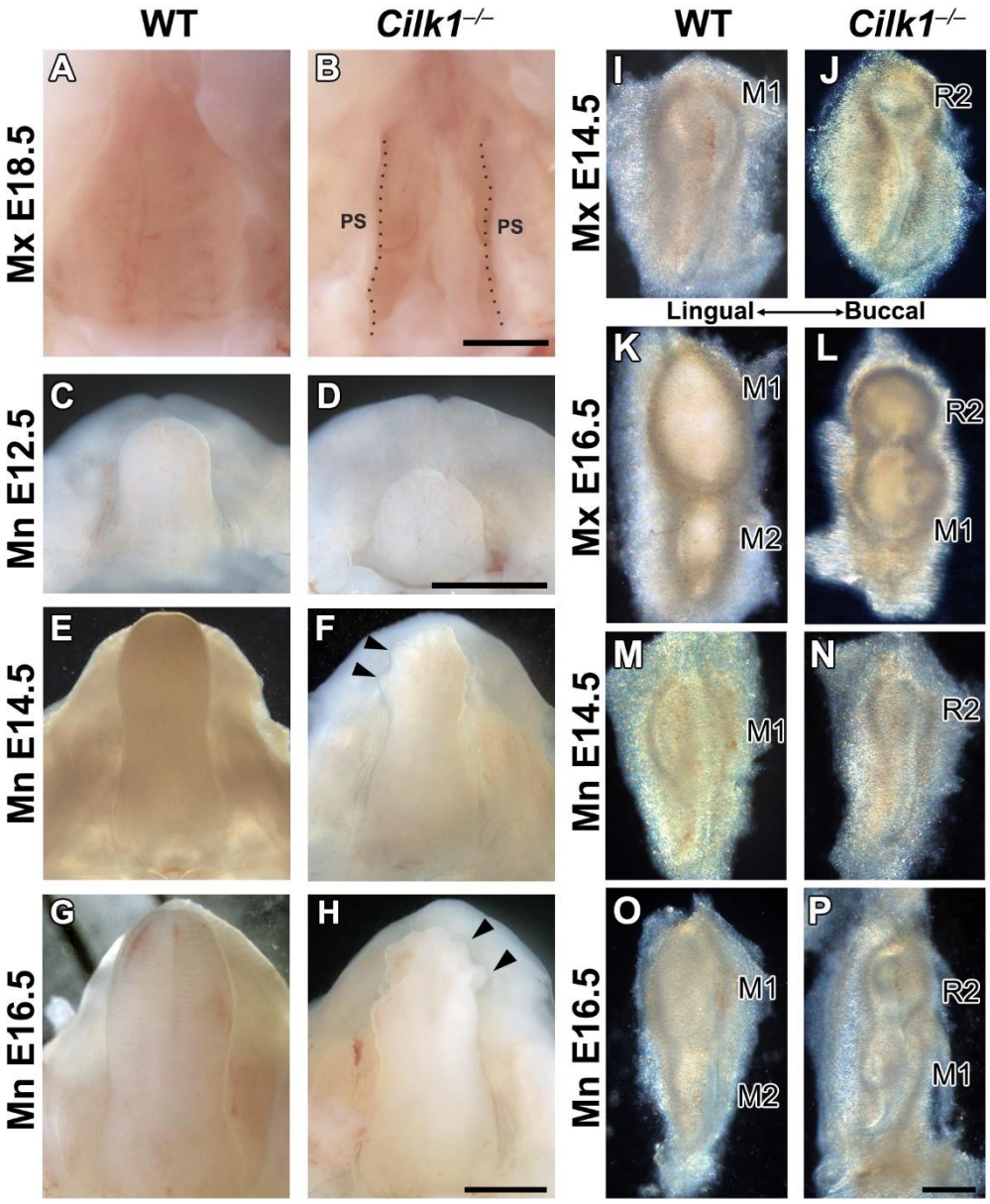

Figure 3. Cleft palate, lobulated tongue and supernumerary molars in *Cilk1*$^{-/-}$ mice

(A) Wild-type mice show fused palatal shelves at E18. (B) *Cilk1*$^{-/-}$ mice show cleft palate at E18.5 with two separated palatal shelves. (D) From E12.5, *Cilk1*$^{-/-}$ embryo mandible (Mn) shows a decreased size of tongue compared to wild-type mandible. (F, H) Globular shaped and shortened tongue tip (black arrowheads) is observed in *Cilk1* mutant mouse from E14 (I–P) tooth germs dissected from maxilla (Mx) and mandible (Mn) of WT and *Cilk1*$^{-/-}$ mice at E14.5 and E16.5. (J, N) Supernumerary tooth (R2) of *Cilk1*$^{-/-}$ mice is smaller in size than first molar (M1) of wild-type (WT) mice in both Mx and Mn. (L, P) The persistent presence of R2 and the reduced size of M1 are consistently observed in *Cilk1*$^{-/-}$ mice after bell stage. Scale bars, A–H: 1mm, I–P: 0.25mm

3. *Cilk1*$^{-/-}$ mice displayed decreased size of molar.

Since *Cilk1*$^{-/-}$ mice shows neonatal lethality, the last time point to study tooth development is PN0. To conduct morphological analysis of teeth in *Cilk1*$^{-/-}$ mice, we compared micro-computed tomography (micro-CT) images of *Cilk1*$^{-/-}$ and wild-type mice (Fig. 4A, B). In frontal sections of micro-CT, one supernumerary tooth was formed in each of four jaw quadrants of *Cilk1*$^{-/-}$ mice. In addition, cleft palate and lobulated tongue were observed again in micro-CT sections.

In histologic sections, R2 of *Cilk1*$^{-/-}$ mice in both maxilla and mandible was different in shape of dental epithelium from M1 of wild-type mice at E15.5. In particular, the length of buccal dental epithelium was short in R2. There was no significant difference in size between R2 of *Cilk1*$^{-/-}$ mice and M1 in wild-type mice at E15.5, while the size of R2 was small than M1 in both maxilla and mandible at PN0 (Fig. 4G, H, K, L). Additionally, in mandibular R2, a short and thickened appearance of dental lamina was also observed (Fig. 4L) wild-type, which lay the mandible tooth germ closer to the oral epithelium. Furthermore, ameloblast and odontoblast were well differentiated in wild-type mice, whereas they were less differentiated in *Cilk1*$^{-/-}$ mice (Fig. 4K', L').

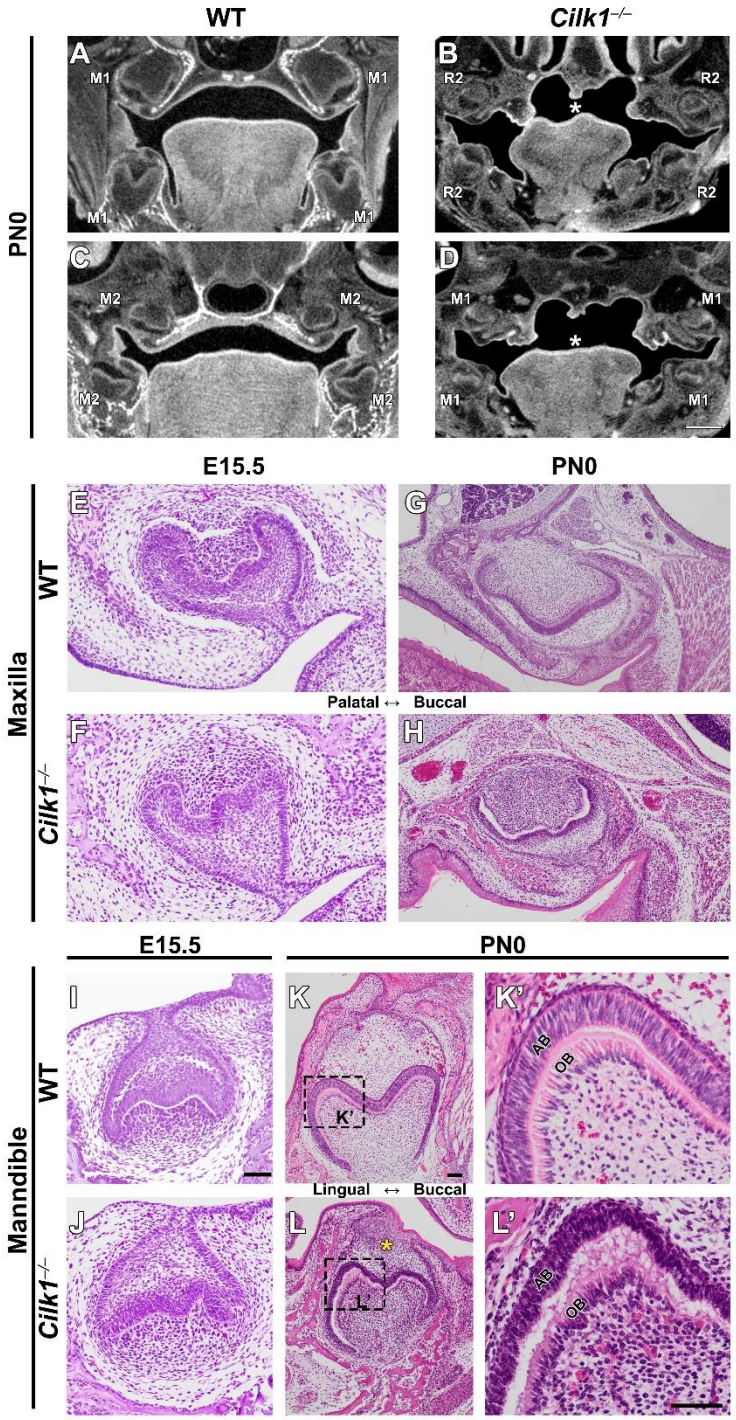

Figure 4. Supernumerary molars in *Cilk1*$^{-/-}$ mice

(A−D) Frontal micro-CT sections of (A, C) wild-type M1 and (B, D) *Cilk1*$^{-/-}$ R2 at postnatal day (PN) 0. Cleft palate and lobulated tongue are observed in *Cilk1*$^{-/-}$ mice in micro-CT sections at the level of R2 and M1 (white asterisk in B and D). (E−L') Frontal histologic sections of M1 of wild-type and *Cilk1*$^{-/-}$ mice. *Cilk1*$^{-/-}$ mandibular R2 shows short and thick dental lamina (yellow asterisk in L). (K', L') Ameloblasts (AB) and odontoblasts (OB) are well differentiated in M1 of wild-type mice but not in the R2 of the *Cilk1*$^{-/-}$ mice at PN0. Scale bars: A−D: 500 ㎛, E−L': 50 ㎛.

4. *Cilk1* deficiency resulted in decrease in the anteroposterior length in snout, mandible, and incisors.

A decrease in tooth size in *Cilk1*$^{-/-}$ mice at PN0 was observed not only in molars but also in incisors. The anteroposterior length of the incisor in *Cilk1*$^{-/-}$ mice were approximately half of the anteroposterior length in wild-type mice in both maxilla and mandible (Fig. 5E). This indicates that the development of molar and incisor was delayed in *Cilk1*$^{-/-}$ mice. Likewise, the snout length and anteroposterior length of the mandible was shorter in *Cilk1*$^{-/-}$ mice than in wild-type mice (Fig. 5F−J). Taken together, these results indicate that the *Cilk1* involve not only in the growth of the incisor but also in the growth of maxilla and mandible bones.

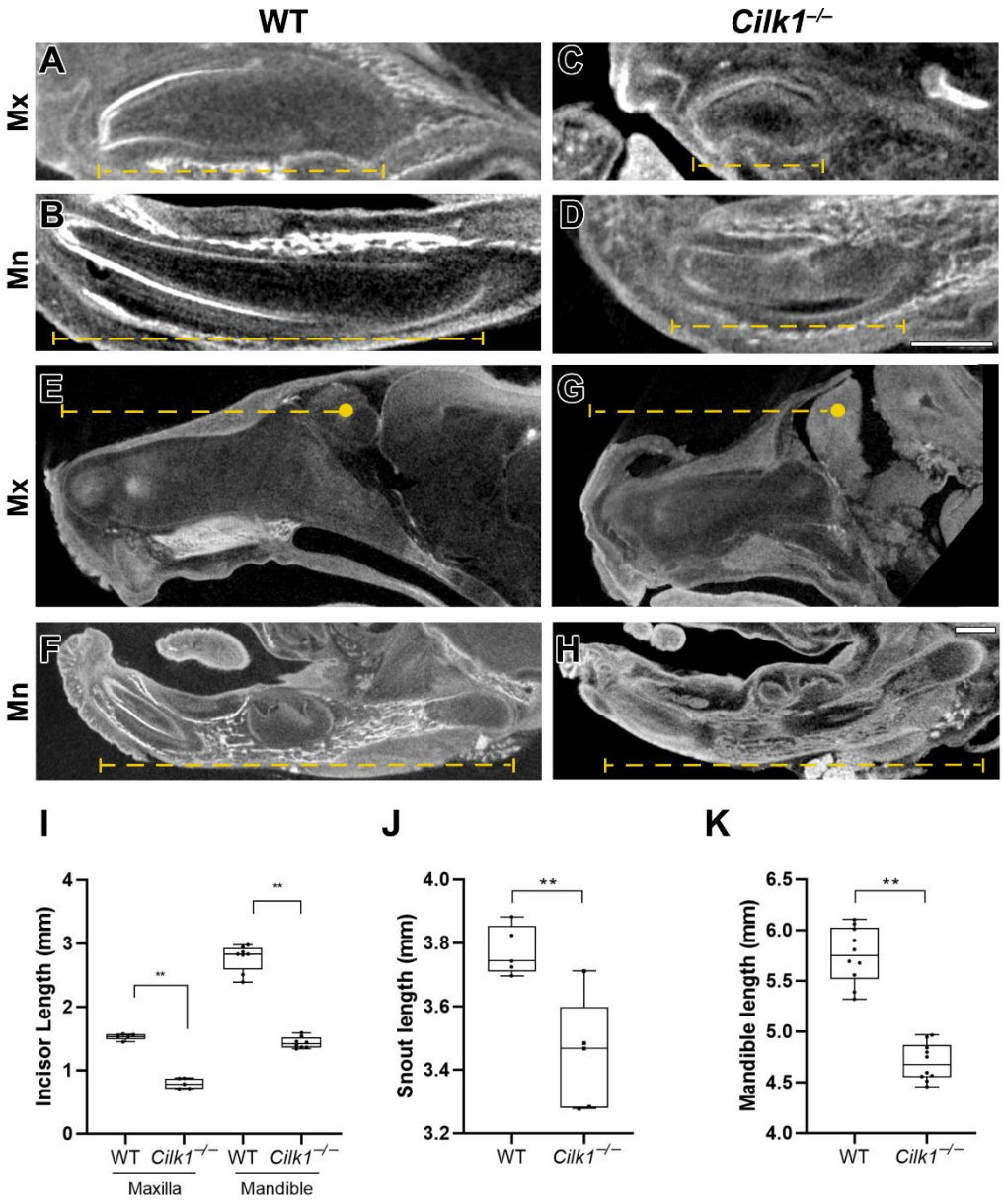

Figure 5. Decrease in the anteroposterior length in snout, mandible, and incisors of *Cilk1*$^{-/-}$ mice at postnatal day 0

(A−D) Maxilla and mandible incisor teeth of wild-type (A, B) and *Cilk1*$^{-/-}$ (C, D) in micro-computed tomography section. (C, D) In contrast to the incisors of wild-type mice, reduced incisor size and uneven labial side curvature can be observed in *Cilk1*$^{-/-}$. (I) At the PN 0 stage, length of the *Cilk1*$^{-/-}$ incisor from the cervical loop to the incisor tip is decreased significantly. (E−H) Maxilla and mandible anteroposterior length of wild-type (E, F) and *Cilk1*$^{-/-}$ (G, H) were measured on sagittal axis. Decreased snout length (J) from interpupillary axis (yellow circle) to nasal cartilage tip and mandible length (K) from condyle to end of mandible bone was observed in *Cilk1*$^{-/-}$. (I: incisor lengths are measured from at least 5 incisors from four or more embryos for each genotype, J: wild-type maxilla, n = 5; *Cilk1*$^{-/-}$ maxilla, n = 5; wild-type mandible, n = 10; *Cilk1*$^{-/-}$ mandible, n = 10). $^{**}p < 0.01$

5. Tooth germs of *Cilk1*$^{-/-}$ mice formed calcified teeth.

Since the *Cilk1*$^{-/-}$ mice are neonatal lethal, it is impossible to identify the final form of teeth. To confirm the role of *Cilk1* gene in the later events of tooth development, such as enamel, dentin, cementum and periodontal ligament formation, transplantation of mandibular developing molars at the cap stage of WT and *Cilk1*$^{-/-}$ mice into the subcapsular layer of kidney of adult male mice was performed. At 4 weeks after transplantation, the fully calcified teeth were formed from developing molars of both WT and *Cilk1*$^{-/-}$ mice (Fig. 6A, B). In micro-CT sections, enamel, dentin, alveolar bones were well observed in all teeth formed from wild-type and *Cilk1*$^{-/-}$ tooth germs (Fig. 6G). In histologic sections, dentinal tubules in dentin, pre-dentin, and odontoblasts in dental pulp were clearly observed in wild-type and *Cilk1*$^{-/-}$ teeth. Considering these results, *Cilk1* affects tooth patterning and morphogenesis, but does not affect the formation of enamel and dentin. These results suggest that ameloblast and odontoblast can be differentiated without *Cilk1* in developing tooth.

Although the tooth structures were similar, two major differences were found between wild-type calcified teeth and *Cilk1*$^{-/-}$ calcified teeth. First, root length was shorter in *Cilk1*$^{-/-}$ teeth (Fig. 6G, H). Second, the tooth pattern was different (Fig. 6C, D). In wild-type calcified teeth, the size of the teeth decreased from left to right (Fig. 6A, C), whereas in *Cilk1*$^{-/-}$ calcified teeth, the central tooth was the largest (Fig. 6B, D). This is consistent with the tooth pattern commonly seen in mutant mice that showed supernumerary tooth formation (Tian et al. 2017; Seo et al. 2018; Ohazama et al. 2009) and the pattern seen in

Cilk1$^{-/-}$ mice at E16.5 (Fig. 3L, P). These results indicate that R2 in *Cilk1*$^{-/-}$ mouse embryos survived to form calcified teeth.

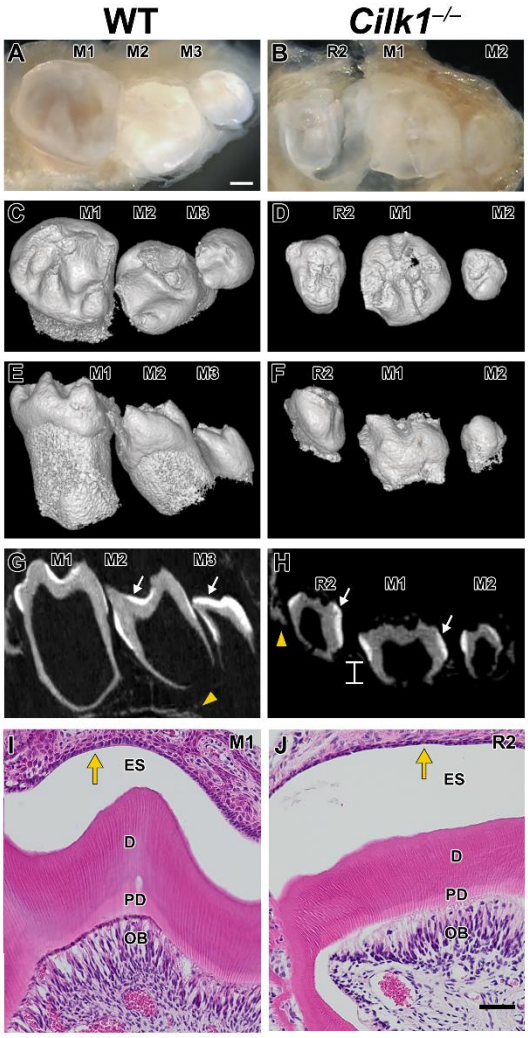

Figure 6. Calcified teeth formed by mandibular E14.5 tooth germs of *Cilk1*$^{-/-}$ mice at 4 weeks after being transplanted into the subcapsular layer of kidney

(A, B) Calcified teeth and alveolar bone dissected from the kidney at 4 weeks after being transplanted into the renal subcapsular layer of adult mice. (C−F) Three-dimensionally (3D) reconstructed calcified teeth after removal of alveolar bone in occlusal view (C, D)

and sagittal view (E, F) of the wild-type and *Cilk1*$^{-/-}$ teeth. The wild-type and *Cilk1*$^{-/-}$ teeth show calcified enamel (arrows in G and H), dentin, well-differentiated odontoblasts in dental pulp, and protective stage ameloblasts (arrows in I and J). Calcified teeth are well surrounded by alveolar bone (yellow arrowheads in G and H). Scale bars: A–H: 250 μm, I–J: 50 μm

6. Ciliary length was decreased in the developing tooth germ of *Cilk1*$^{-/-}$ mice

To confirm whether the tooth pattern change was due to alterations in the frequency and length of primary cilia were measured in the frontal sections of developing molars at E15.5 (Fig. 7A, B). The frequency of primary cilia detected by primary cilia specific marker, Arl13b, was significantly reduced in the dental epithelium and mesenchyme, while cilia length was significantly increased in dental epithelium and mesenchyme of *Cilk1*$^{-/-}$ tooth germ (Fig. 7F). These results indicate that *Cilk1* regulates the length and frequency of primary cilia during tooth development, and that abnormalities in primary cilia in teeth can cause significant changes in the tooth patterns.

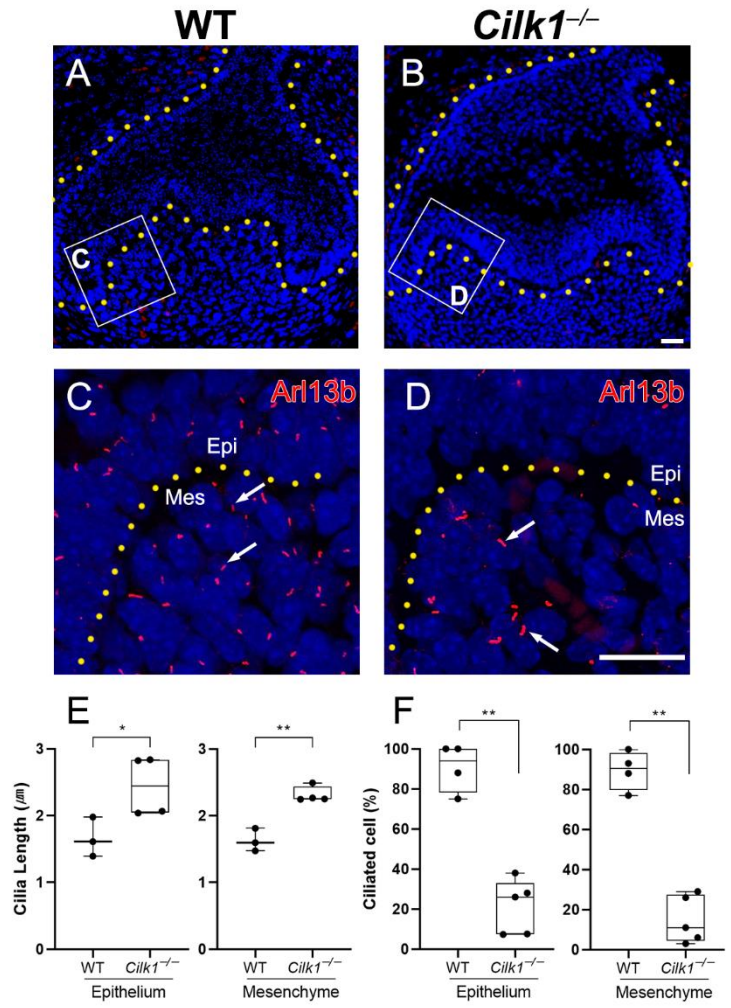

Figure 7. Alterations in the length and frequency of primary cilia in developing teeth of *Cilk1*$^{-/-}$ mice

(A-D) Immunohistochemistry of Arl13b, cilia marker in cap stage tooth germ. Quantification of cilia body length in the developing tooth germ of wild-type M1 and *Cilk1*$^{-/-}$ R2. (E) Primary cilia are significantly elongated in both the dental epithelium and

mesenchyme of R2. (F) Percentage of ciliated dental epithelial and mesenchymal cells are significantly decreased in R2 of *Cilk1*$^{-/-}$ mice. *$p < 0.05$, **$p < 0.01$ Scale bar: A−D 20 ㎛.

7. Hedgehog signaling activity was down-regulated in the developing tooth germ.

In order to investigate the molecular changes underlying alterations in tooth patterns of *Cilk1*$^{-/-}$ mice, RNA sequencing was performed in maxillary molars at multiple developmental stages, which are crucial stages for tooth pattern formation (Cho et al. 2011). In Gene ontology (GO) enrichment analysis with the downregulated genes, 'Smoothened binding', 'Hedgehog receptor activity' and 'Hedgehog family protein binding' were the most significant enriched in molecular function (Fig. 8B). A significant down-regulation of Hedgehog pathway target genes, including *Gli1*, *Sostdc1,* and *Ptch1*, was observed in *Cilk1*$^{-/-}$ mice compare to wild-type mice at E13.5, E14.5, and E15.5 (Fig. 8C). In the list of up-regulated or down-regulated genes in *Cilk1*$^{-/-}$ mice, genes in primary cilia formation and other signaling pathways were not included.

These findings suggest that the crucial role of *Cilk1* in modulating the Hedgehog pathway during tooth development, shedding light on the down-regulation of Hedgehog signaling pathway as a key factor contributing to the alterations in tooth patterns of *Cilk1*$^{-/-}$ mice (Fig. 8).

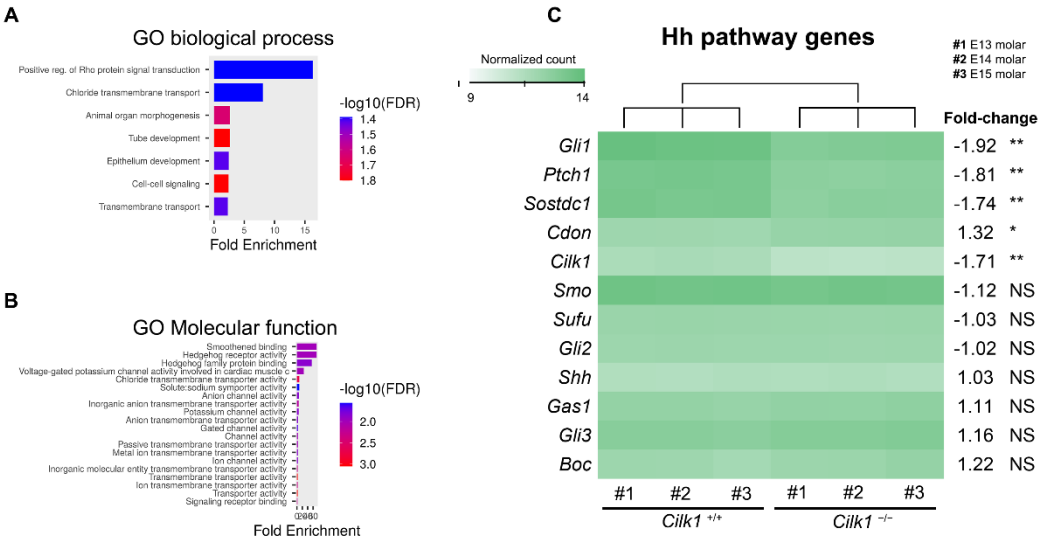

Figure 8. Alterations in gene expression level in developing molars of *Cilk1*$^{-/-}$ mice

(A, B) Gene ontology enrichment analysis with the significantly downregulated genes showing the most enriched GO biological process and GO molecular function terms. All significantly enriched molecular function terms are associated with Hedgehog pathway. (C) Heatmaps display the normalized count levels of genes in the *Cilk1*$^{-/-}$ and wild-type maxilla tooth germs' developing stages of RNA sequencing analysis. Among Hedgehog related genes, *Shh* targets genes including *Gli1, Ptch1, Sostdc1* were significantly downregulated in *Cilk1*$^{-/-}$ mice.

Table 1. Upregulated genes in *Cilk1*$^{-/-}$ mice compared to *Cilk1*$^{+/+}$ mice in maxillary tooth germ at E13.5, 14.5, 15.5 (fold change > 1.5, P adj < 0.05)

Gene id	Gene name	Gene description	Fold change	P adj
ENSMUSG00000019852	*Arfgef3*	ARFGEF family member 3	2.50449	0.049612
ENSMUSG00000030607	*Acan*	aggrecan	3.24530	0.034358
ENSMUSG00000070469	*Adamtsl3*	ADAMTS-like 3	2.09266	0.002244
ENSMUSG00000064294	*Aox3*	aldehyde oxidase 3	2.15780	0.021854
ENSMUSG00000021388	*Aspn*	asporin	1.54526	0.000621
ENSMUSG00000058914	*C1qtnf3*	C1q and tumor necrosis factor related protein 3	1.77789	0.000008
ENSMUSG00000030669	*Calca*	calcitonin/calcitonin-related polypeptide, alpha	1.78114	0.000937
ENSMUSG00000039145	*Camk1d*	calcium/calmodulin-dependent protein kinase ID	1.56637	0.000784
ENSMUSG00000052353	*Cemip*	cell migration inducing protein, hyaluronan binding	2.53610	0.001061
ENSMUSG00000026147	*Col9a1*	collagen, type IX, alpha 1	2.04133	0.000325
ENSMUSG00000021508	*Cxcl14*	chemokine (C-X-C motif) ligand 14	1.67597	0.008944
ENSMUSG00000068373	*D430041D05Rik*	RIKEN cDNA D430041D05 gene	2.13958	0.000596
ENSMUSG00000031285	*Dcx*	doublecortin	1.84100	0.003041
ENSMUSG00000047842	*Diras2*	DIRAS family, GTP-binding RAS-like 2	1.69663	0.000021
ENSMUSG00000052572	*Dlg2*	discs large MAGUK scaffold protein 2	1.54910	0.003139
ENSMUSG00000005237	*Dnah2*	dynein, axonemal, heavy chain 2	1.76712	0.005147
ENSMUSG00000019936	*Epyc*	epiphycan	3.70222	0.025796
ENSMUSG00000038233	*Fam198a*	family with sequence similarity 198, member A	1.96281	0.012527
ENSMUSG00000074505	*Fat3*	FAT atypical cadherin 3	1.67634	0.000060
ENSMUSG00000021943	*Gdf10*	growth differentiation factor 10	1.73175	0.000165
ENSMUSG00000093587	*Gm20554*	predicted gene, 20554	1.98376	0.000002
ENSMUSG00000002771	*Grin2d*	glutamate receptor, ionotropic, NMDA2D (epsilon 4)	1.80113	0.021663
ENSMUSG00000046711	*Hmga1*	high mobility group AT-hook 1	1.52274	0.004886
ENSMUSG00000032269	*Htr3a*	5-hydroxytryptamine (serotonin) receptor 3A	1.69408	0.042466
ENSMUSG00000068154	*Insm1*	insulinoma-associated 1	5.53459	0.000163
ENSMUSG00000032243	*Itga11*	integrin alpha 11	1.94045	0.003128
ENSMUSG00000040164	*Kcns1*	K+ voltage-gated channel, subfamily S, 1	2.17165	0.007749

ENSMUSG00000046834	*Krt1*	keratin 1	1.69418	0.005666
ENSMUSG00000020140	*Lgr5*	leucine rich repeat containing G protein coupled receptor 5	1.59217	0.015226
ENSMUSG00000092341	*Malat1*	metastasis associated lung adenocarcinoma transcript 1 (non-coding RNA)	1.51081	0.000024
ENSMUSG00000030218	*Mgp*	matrix Gla protein	1.53236	0.019779
ENSMUSG00000040280	*Ndufa4l2*	Ndufa4, mitochondrial complex associated like 2	1.73475	0.003139
ENSMUSG00000022055	*Nefl*	neurofilament, light polypeptide	3.87921	0.007237
ENSMUSG00000055409	*Nell1*	NEL-like 1	1.57582	0.028180
ENSMUSG00000028341	*Nr4a3*	nuclear receptor subfamily 4, group A, member 3	2.95213	0.036599
ENSMUSG00000033768	*Nrxn2*	neurexin II	1.69499	0.042466
ENSMUSG00000103567	*Pcdhga5*	protocadherin gamma subfamily A, 5	1.83061	0.042466
ENSMUSG00000041577	*Prelp*	proline arginine-rich end leucine-rich repeat	1.54589	0.002964
ENSMUSG00000050558	*Prokr2*	prokineticin receptor 2	1.93883	0.042466
ENSMUSG00000027864	*Ptgfr*	prostaglandin F2 receptor negative regulator	1.57723	0.001860
ENSMUSG00000060735	*Rxfp3*	relaxin family peptide receptor 3	2.12978	0.000534
ENSMUSG00000038738	*Shank1*	SH3 and multiple ankyrin repeat domains 1	1.75439	0.000023
ENSMUSG00000030257	*Srgap3*	SLIT-ROBO Rho GTPase activating protein 3	1.52258	0.000073
ENSMUSG00000035431	*Sstr1*	somatostatin receptor 1	1.86944	0.019696
ENSMUSG00000052415	*Tchh*	trichohyalin	2.07543	0.006277
ENSMUSG00000043592	*Unc5c*	unc-5 family C-terminal like	1.50624	0.003041
ENSMUSG00000049641	*Vgll2*	vestigial like family member 2	6.14820	0.015227
ENSMUSG00000002266	*Zim1*	zinc finger, imprinted 1	1.89058	0.000000

Table 2. Downregulated genes in *Cilk1*$^{-/-}$ mice compared to *Cilk1*$^{+/+}$ mice in maxillary tooth germ at E13.5, 14.5, 15.5 (fold change > 1.5, P adj < 0.05)

Gene id	Gene name	Gene description	Fold change	P adj
ENSMUSG00000022449	*Adamts20*	a disintegrin-like and metallopeptidase (reprolysin type) with thrombospondin type 1 motif, 20	-1.547635	0.000312
ENSMUSG00000031659	*Adcy7*	adenylate cyclase 7	-1.826641	0.000000
ENSMUSG00000037860	*Aim2*	absent in melanoma 2	-2.024405	0.014334
ENSMUSG00000030909	*Anks4b*	ankyrin repeat and sterile alpha motif domain containing 4B	-4.085682	0.014214
ENSMUSG00000031654	*Cbln1*	cerebellin 1 precursor protein	-1.834697	0.000596
ENSMUSG00000032572	*Col6a4*	collagen, type VI, alpha 4	-3.523570	0.000603
ENSMUSG00000030905	*Crym*	crystallin, mu	-1.524970	0.036550
ENSMUSG00000019278	*Dpep1*	dipeptidase 1 (renal)	-2.728631	0.009293
ENSMUSG00000031383	*Dusp9*	dual specificity phosphatase 9	-1.646399	0.042466
ENSMUSG00000024053	*Emilin2*	elastin microfibril interfacer 2	-1.530719	0.009842
ENSMUSG00000038402	*Foxf2*	forkhead box F2	-2.433246	0.000000
ENSMUSG00000097084	*Foxl1*	forkhead box L1	-2.497854	0.000519
ENSMUSG00000091387	*Gcnt4*	glucosaminyl (N-acetyl) transferase 4, core 2 (beta-1,6-N-acetylglucosaminyltransferase)	-2.507801	0.000325
ENSMUSG00000046167	*Gldn*	gliomedin	-2.745938	0.000084
ENSMUSG00000025407	*Gli1*	GLI-Kruppel family member GLI1	-1.917435	0.000000
ENSMUSG00000001985	*Grik3*	glutamate receptor, ionotropic, kainate 3	-1.878303	0.031720
ENSMUSG00000003283	*Hck*	hemopoietic cell kinase	-1.756573	0.014255
ENSMUSG00000039628	*Hs3st6*	heparan sulfate (glucosamine) 3-O-sulfotransferase 6	-2.120624	0.000084
ENSMUSG00000009828	*Cilk1*	ciliogenesis associated kinase 1	-1.711951	0.000000
ENSMUSG00000055675	*Kbtbd11*	kelch repeat and BTB (POZ) domain containing 11	-1.556939	0.013575
ENSMUSG00000026840	*Lamc3*	laminin gamma 3	-1.814345	0.000016
ENSMUSG00000038244	*Mical2*	microtubule associated monooxygenase, calponin and LIM domain containing 2	-1.581152	0.000595
ENSMUSG00000040138	*Ndp*	Norrie disease (pseudoglioma) (human)	-2.643263	0.000312
ENSMUSG00000000120	*Ngfr*	nerve growth factor receptor (TNFR superfamily, member 16)	-1.789557	0.000000
ENSMUSG00000059991	*Nptx2*	neuronal pentraxin 2	-2.366535	0.007237
ENSMUSG00000020902	*Ntn1*	netrin 1	-1.820603	0.000030

ENSMUSG00000102697	*Pcdhac2*	protocadherin alpha subfamily C, 2	-1.519936	0.004307
ENSMUSG00000102748	*Pcdhgb2*	protocadherin gamma subfamily B, 2	-1.569625	0.021979
ENSMUSG00000045573	*Penk*	preproenkephalin	-1.546431	0.003041
ENSMUSG00000063446	*Plppr1*	phospholipid phosphatase related 1	-2.153345	0.000040
ENSMUSG00000021466	*Ptch1*	patched 1	-1.810172	0.000000
ENSMUSG00000028681	*Ptch2*	patched 2	-1.581137	0.000020
ENSMUSG00000024565	*Sall3*	spalt like transcription factor 3	-2.723254	0.012738
ENSMUSG00000057969	*Sema3b*	sema domain, immunoglobulin domain (Ig), short basic domain, secreted, (semaphorin) 3B	-1.793651	0.007237
ENSMUSG00000038264	*Sema7a*	sema domain, immunoglobulin domain (Ig), and GPI membrane anchor, (semaphorin) 7A	-1.810214	0.000014
ENSMUSG00000024935	*Slc1a1*	solute carrier family 1 (neuronal/epithelial high affinity glutamate transporter, system Xag), member 1	-5.037450	0.000009
ENSMUSG00000021136	*Smoc1*	SPARC related modular calcium binding 1	-2.144359	0.000000
ENSMUSG00000036169	*Sostdc1*	sclerostin domain containing 1	-1.743712	0.000000
ENSMUSG00000031253	*Srpx2*	sushi-repeat-containing protein, X-linked 2	-1.639351	0.042466
ENSMUSG00000032327	*Stra6*	stimulated by retinoic acid gene 6	-1.993083	0.012527
ENSMUSG00000022658	*Tagln3*	transgelin 3	-1.731316	0.003911
ENSMUSG00000000782	*Tcf7*	transcription factor 7, T cell specific	-1.604772	0.001789
ENSMUSG00000032011	*Thy1*	thymus cell antigen 1, theta	-2.076785	0.000034
ENSMUSG00000032554	*Trf*	transferrin	-1.552167	0.007493
ENSMUSG00000030351	*Tspan11*	tetraspanin 11	-1.741660	0.000002

8. Different tooth patterning in more severe impaired Hedgehog pathway

The decreased Hedgehog signaling activity and defects in primary cilia observed in *Cilk1*$^{-/-}$ mice suggest that Hedgehog signaling is impaired in Shh-responsive cells, primarily in the dental mesenchyme, rather than in Shh-producing cells, which are located in the enamel knot. Conversely, PCS1−MRCS1$^{\triangle/\triangle}$ mouse has been identified as having reduction in *Shh* expression within Hedgehog-producing cells due to the deletion of oral-specific Shh enhancers. PCS1−MRCS1$^{\triangle/\triangle}$ mice are viable and show calcified supernumerary teeth in maxilla and mandible. In order to further reduce the Hedgehog signaling activity in tooth germs, PCS1−MRCS1$^{\triangle/\triangle}$ mice were crossed with *Cilk1*$^{-/-}$mice to generate *Cilk1*$^{-/-}$;PCS1−MRCS1$^{\triangle/\triangle}$ mice.

Similar to *Cilk1*$^{-/-}$ mice, cleft palate and lobulated tongue were observed in *Cilk1*$^{-/-}$;PCS1−MRCS1$^{\triangle/\triangle}$ mice at E16 (Fig. 9C, F). Also, the expression pattern of *Shh* in tooth germs in *Cilk1*$^{-/-}$;PCS1−MRCS1$^{\triangle/\triangle}$ mice was similar to that of *Cilk1*$^{-/-}$mice but different from that wild-type mice. This result suggests the supernumerary tooth formation in both maxilla and mandible of *Cilk1*$^{-/-}$;PCS1−MRCS1$^{\triangle/\triangle}$ mice.

Due to the lethality of *Cilk1*$^{-/-}$ and *Cilk1*$^{-/-}$;PCS1−MRCS1$^{\triangle/\triangle}$ mice at birth,

tooth pattern changes were examined at PN 0 (Fig. 10). Supernumerary teeth were observed in the maxilla and mandible of *Cilk1*$^{-/-}$, PCS1−MRCS1$^{\triangle/\triangle}$, and *Cilk1*$^{-/-}$;PCS1−MRCS1$^{\triangle/\triangle}$ mice. Additionally, the *Cilk1*$^{-/-}$;PCS1−MRCS1$^{\triangle/\triangle}$ mice exhibited molar fusion in the maxilla, but not in the mandible (Fig. 10G, g', g'').

PCS1−MRCS1$^{\triangle/\triangle}$ mice showed supernumerary tooth pattern at a rate of 41% in maxilla and 34% in mandible of PCS1−MRCS1$^{\triangle/\triangle}$. In *Cilk1*$^{-/-}$ mice, supernumerary tooth pattern occurred at a rate of 100% in both maxilla and mandible. In *Cilk1*$^{-/-}$;PCS1−MRCS1$^{\triangle/\triangle}$ mice the supernumerary tooth pattern and the molar fusion appeared at a rate of 52% and 48%, respectively in maxilla, while the mandible showed the supernumerary tooth pattern only (Fig. 12A). Interestingly, the ratio of R2 to M1 in mesiodistal length was different among the three types of mutant mice showing the supernumerary tooth pattern. In *Cilk1*$^{-/-}$;PCS1−MRCS1$^{\triangle/\triangle}$ mice, the mesiodistal length of R2 was occasionally larger than that of the M1 during the formation of supernumerary molars. Among the maxillary tooth phenotypes of *Cilk1*$^{-/-}$;PCS1−MRCS1$^{\triangle/\triangle}$ mice, 38% exhibited R2 > M1, while in the mandible, 64% and 36% of cases exhibited R2 > M1 and R2 < M1, respectively. The R2/M1 ratio was significantly increased in *Cilk1*$^{-/-}$;PCS1−MRCS1$^{\triangle/\triangle}$ mice compared to *Cilk1*$^{-/-}$ mice and PCS1−MRCS1$^{\triangle/\triangle}$

mice. This phenomenon was observed in both maxilla and mandible (Fig. 12B). In *Cilk1*$^{-/-}$;PCS1−MRCS1$^{\triangle/\triangle}$ mice, the size of R2 was nearly identical to M1, with occasional instances of R2 being larger than M1. These findings suggest that the R2/M1 ratio is associated with the level of Hedgehog signaling activity, highlighting the close relationship between *Cilk1* and the Hedgehog pathway in tooth pattern formation.

To investigate the dependence of tooth pattern changes on Hedgehog activity during development, we employed in situ hybridization to analyze the expression patterns of genes involved in the Wnt-Shh-Sostdc1 negative feedback loop, including *Lef1*, *Ptch1* and *Sostdc1* (Fig. 11). Hematoxylin and eosin staining results showed supernumerary teeth in the mutant group (Fig. 11B,C). In situ hybridization results revealed that *Ptch1* and *Sostdc1* expression was greatly decreased in *Cilk1*$^{-/-}$ and *Cilk1*$^{-/-}$;PCS1−MRCS1$^{\triangle/\triangle}$molars compared to wild-type dental mesenchyme (Fig. 11E-F, H-I). Interestingly, *Lef1* expression was similar between wild-type and mutant molar tooth germs (Fig. 11J−L). This suggests that Shh target genes affect tooth patterning in *Cilk1*$^{-/-}$ and *Cilk1*$^{-/-}$;PCS1−MRCS1$^{\triangle/\triangle}$ embryos during tooth development.

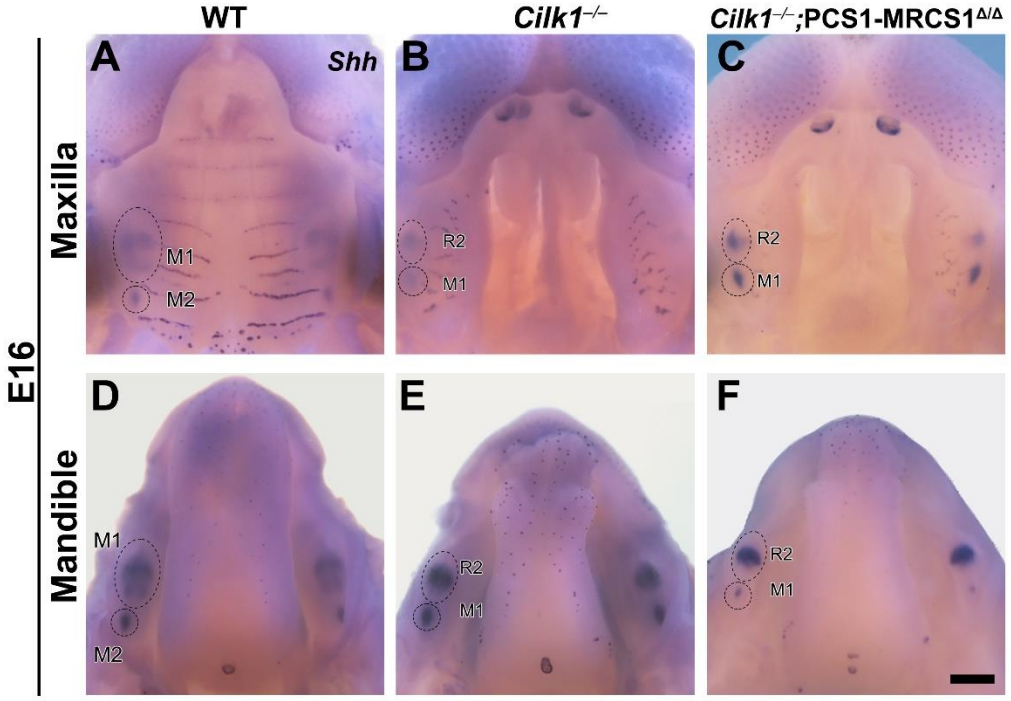

Figure 9. Expression pattern of *Shh* in palatal rugae, tongue papillae, and tooth germs of *Cilk1*$^{-/-}$, and *Cilk1*$^{-/-}$; PCS1−MRCS1$^{\triangle/\triangle}$ mice

(A-F) Visualized mutant phenotypic changes by whole mount in situ hybridization using *Shh* mRNA on WT, *Cilk1*$^{-/-}$, *Cilk1*$^{-/-}$;PCS1−MRCS1$^{\triangle/\triangle}$ mice maxilla and mandible at E16. Decreased size of first molar (M1) depends on changes in lower Hedgehog signaling level. Scale bar: A-F, 500 ㎛.

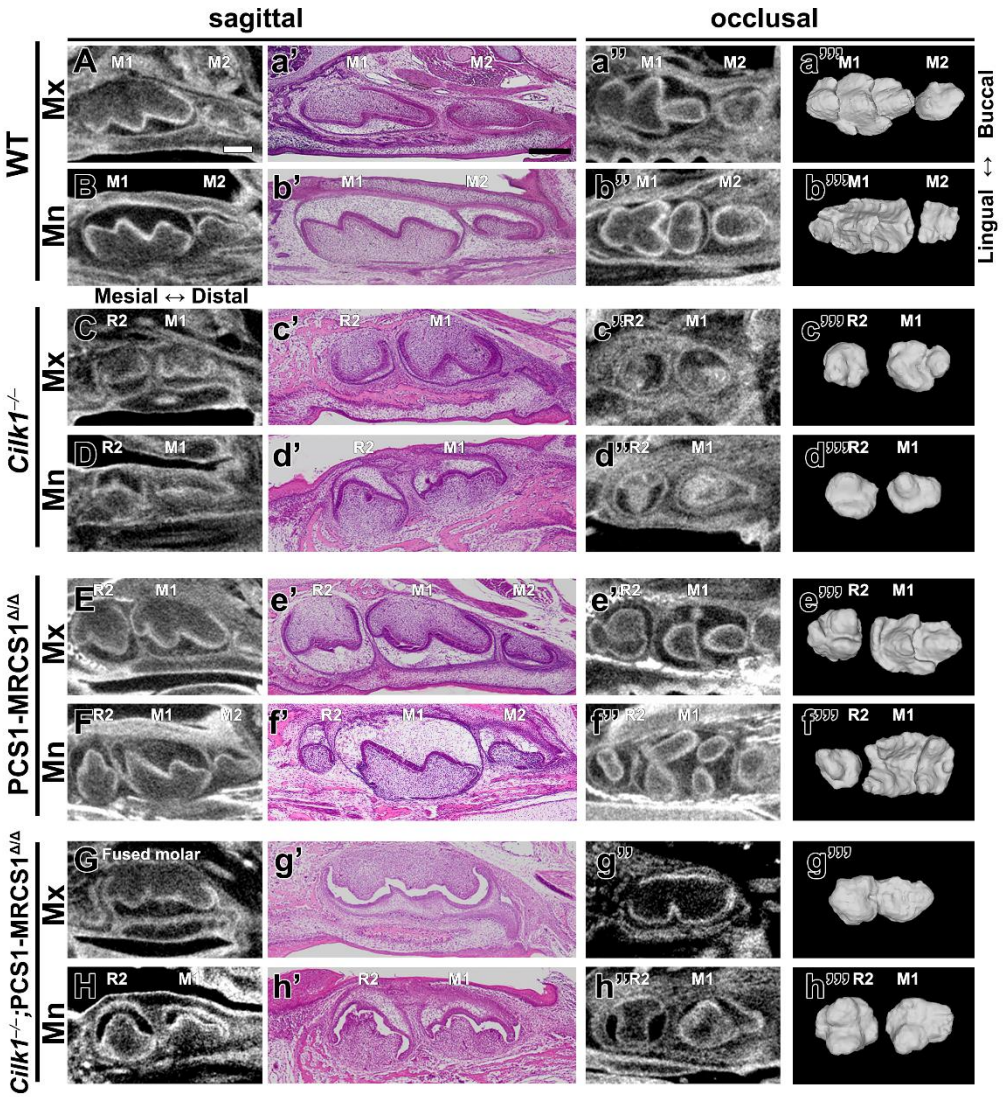

Figure 10. Alterations in tooth pattern of *Cilk1*$^{-/-}$, PCS1−MRCS1$^{\Delta/\Delta}$, and *Cilk1*$^{-/-}$; PCS1−MRCS1$^{\Delta/\Delta}$ mice

Tooth pattering changes at PN0 in wild-type (WT), *Cilk1*$^{-/-}$, PCS1−MRCS1$^{\triangle/\triangle}$, *Cilk1*$^{-/-}$;PCS1−MRCS1$^{\triangle/\triangle}$maxilla and mandible. (A−H) Micro-computed tomography (micro-CT) images showing sagittal view at postnatal day 0 (PN0) mouse. (a' −h') Hematoxylin and Eosin (H&E) staining showing sagittal view of WT, *Cilk1*$^{-/-}$, PCS1−MRCS1$^{\triangle/\triangle}$, *Cilk1*$^{-/-}$;PCS1−MRCS1$^{\triangle/\triangle}$ maxilla and mandible (a'' −h''). Micro-CT images showing occlusal section of WT, *Cilk1*$^{-/-}$, PCS1−MRCS1$^{\triangle/\triangle}$, *Cilk1*$^{-/-}$;PCS1−MRCS1$^{\triangle/\triangle}$ maxilla and mandible (a''' −h'''). 3D reconstructed occlusal view of WT, *Cilk1*$^{-/-}$, PCS1−MRCS1$^{\triangle/\triangle}$, *Cilk1*$^{-/-}$;PCS1−MRCS1$^{\triangle/\triangle}$ maxilla and mandible mouse molar model. (C−d''') In *Cilk1*$^{-/-}$, supernumerary tooth (R2) can be observed on the mesial side of first molar (M1). (c''',d''') On the occlusal view 3d reconstructed model, it can be seen that the cusp formation is disorganized. (e''') PCS1−MRCS1$^{\triangle/\triangle}$ mice shows a cusp pattern in which the lower part of the anterocone was cut off in the Mx first molar. (f''') In PCS1−MRCS1$^{\triangle/\triangle}$ mandible, M1 cusp pattern remains under anteroconid of WT M1. (G−g''') In *Cilk1*$^{-/-}$;PCS1−MRCS1$^{\triangle/\triangle}$ maxilla, fused molar is observed (Fig. 10g'''). In *Cilk1*$^{-/-}$;PCS1−MRCS1$^{\triangle/\triangle}$ mandible, R2 is observed bigger than M1 (n = 14). Scale bar: A−h''', 250 ㎛

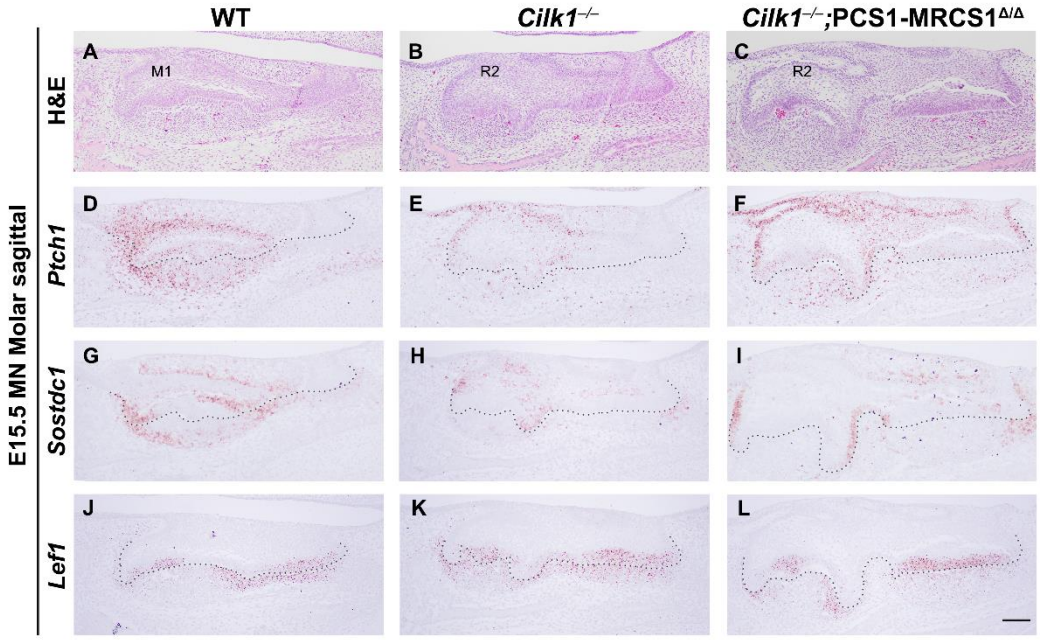

Figure 11. Alterations in the gene expression in developing molars of *Cilk1*$^{-/-}$ and *Cilk1*$^{-/-}$;PCS1−MRCS1$^{\triangle/\triangle}$ mice

(A−C) Hematoxylin and Eosin (H&E) staining showing sagittal view of WT, *Cilk1*$^{-/-}$, *Cilk1*$^{-/-}$;PCS1−MRCS1$^{\triangle/\triangle}$ mandibular molar tooth germ at E15. (D−L) Section in situ hybridization results showing expression patterns of *Ptch1*(D−F), *Sostdc1* (G−I) and *Lef1* (J−L) in the mandibular molar tooth germ of E15.5. Scale bar, A−L: 100㎛

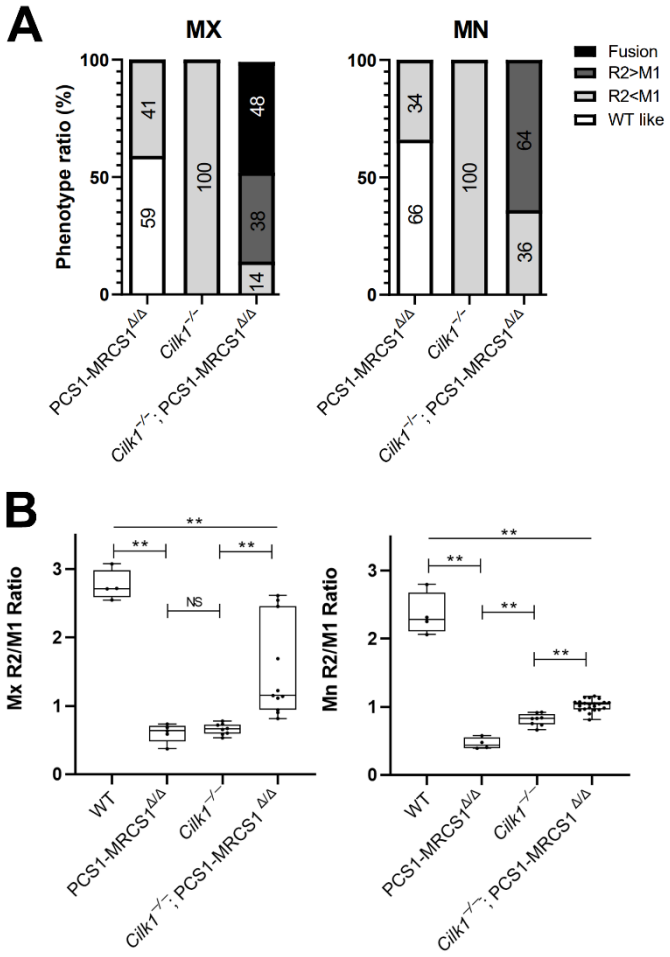

Figure 12. Various tooth pattern depending on Hedgehog signaling activity

(A) Tooth pattern coverage of mutant group with supernumerary teeth. Fused molar is observed only in *Cilk1*$^{-/-}$;PCS1−MRCS1$^{\triangle/\triangle}$ maxilla. (MX: PCS1−MRCS1$^{\triangle/\triangle}$, n = 24; *Cilk1*$^{-/-}$;, n = 20; , *Cilk1*$^{-/-}$;PCS1−MRCS1$^{\triangle/\triangle}$, n = 21) (MN: PCS1−MRCS1$^{\triangle/\triangle}$, n = 26; *Cilk1*$^{-/-}$;, n = 20; , *Cilk1*$^{-/-}$;PCS1−MRCS1$^{\triangle/\triangle}$, n = 22)

(B) A more equal-sized first molar and supernumerary tooth are produced by a change in the lower Hedgehog signaling activity. Statistical comparisons were made using the one-way ANOVA for multiple comparisons. (MX: Wt, n = 4; PCS1−MRCS1$^{\triangle/\triangle}$, n = 5; *Cilk1*$^{-/-}$, n = 8; , *Cilk1*$^{-/-}$;PCS1−MRCS1$^{\triangle/\triangle}$, n = 11) (MN: PCS1−MRCS1$^{\triangle/\triangle}$, n = 4; *Cilk1*$^{-/-}$, n = 8; , *Cilk1*$^{-/-}$;PCS1−MRCS1$^{\triangle/\triangle}$, n = 22) (** $p < 0.01$, NS, nonsignificant.)

IV. DISCUSSION

In line with an earlier study (Hisamoto et al. 2016), primary cilia were observed in the majority of cells in both the dental epithelium and mesenchyme in the present study. It's notable that most cells of the dental epithelium and mesenchyme express *Cilk1* in wild-type mice. Additionally, the increased number of cells lacking primary cilia and the longer length of primary cilia in *Cilk1*-deficient mice suggest that *Cilk1* plays a crucial role in the formation of primary cilia during tooth development.

Molar tooth germ of *Cilk1*$^{-/-}$ mouse embryos at E14.5 forms the calcified teeth and alveolar bone in subcapsular layer of kidney at 4 week after transplantation. *Cilk1*-deficient teeth showed the significantly shorter root length compared to wild-type teeth. This is consistent with previous results that *Ift80,* or *Ift140*-deficient mice show the significantly short roots (Yuan, Cao, and Yang 2019; Li et al. 2018), suggesting an important role of primary cilia in tooth root growth. Additionally, enamel, dentinal tubules, predentin, dentin, alveolar bone and odontoblasts in dental pulp were observed in *Cilk1*$^{-/-}$ teeth, indicating that *Cilk1* might not be essential for ameloblasts and odontoblasts differentiation and their hard tissue formation. However, this observation contrasts with findings from previous tooth germ transplantation study. Tooth germs from *Wnt1-cre;Kif3a*$^{fl/fl}$ mice, when transplanted into the kidney capsule, demonstrated the formation of odontoblasts, but with significantly thin dentin and no enamel (Liu et al. 2014), and *Ift80, Ift88,* or *Ift140*-deficient mice showed thin dentin or enamel formation (Yuan, Cao, and Yang 2019; Li et al. 2018; Kudo et al. 2023). Analyzing the shape of the crown and root,

as well as the volume of hard tissue, in teeth developed through culture in kidney is challenging due to spatial constraints within the renal capsule. Therefore, the precise role of *Cilk1* in hard tissue formation should be further investigated.

In a previous study of tooth patterning using primary cilia-related genes, supernumerary teeth were reported in *Wnt1-cre*/*Ift88*$^{flox/flox}$ mice. In contrast, no changes in tooth patterning were observed in *Krt5-cre*/*Ift88*$^{flox/flox}$ mice and attrition was observed in adult mice (Ohazama et al. 2009; Kudo et al. 2023). These results suggest that primary cilia-related genes in the mesenchyme may be more involved in tooth pattern. The precise dental epithelial-mesenchymal tissue specific CILK1 function in the interaction between Shh producing-responding cells should be investigated using a multiple-model system in further researches.

The importance of primary cilia in the development of craniofacial structure is well known, since many craniofacial defects are caused by loss of primary cilia-related genes in human and mice. In human, mutation in *EVC, EVC2, IFT88, KIF3A, OFD1,* or *IFT121*, induces cleft lip, cleft palate, oligodontia, or supernumerary tooth (Dodge and Kernohan 1967; Curry and Hall 1979; Bureau et al. 2014; Susami et al. 1999; Baujat and Le Merrer 2007; Levin et al. 1977). In mice, deletions in *Evc*, *Evc2*, *Fuz*, *Ift88*, or *Kif3a* genes often lead to a combination of cleft palate, tongue agenesis, mandibular hypoplasia, and supernumerary molars (Ohazama et al. 2009; Tian et al. 2017; Brugmann et al. 2010; Yuan et al. 2017; Nakatomi et al. 2013; Zhang et al. 2022; Zhang et al. 2011). In *Cilk1*-deficient mice, cleft palate and lobulated tongue have already been reported (Moon et al.

2014) and supernumerary teeth were discovered for the first time in the present study.

It has been suggested that mutations in primary cilia-related genes lead to similar phenotypic changes because primary cilia are specialized for Hedgehog signaling pathway (Goetz and Anderson 2010; Dorn, Hughes, and Rohatgi 2012; Zhang et al. 2022; Huangfu et al. 2003; Liu et al. 2014). A close relationship between *Cilk1* and Hedgehog signaling has also already been identified in various organs like central nervous system, smooth muscle patterning, and palatal fusion (Chaya et al. 2014; Yang et al. 2021; Shin et al. 2019). In the present study, the significant reduction in Hedgehog signaling activity observed within in tooth germs of *Cilk1*-deficient mice confirms a close interrelation between *Cilk1*, primary cilia functionality, and Hedgehog signaling during tooth development.

Various tooth patterns have been created depending on the activity of Hedgehog signaling. PCS1−MRCS1$^{\triangle/\triangle}$ mice and MRCS1$^{\triangle/\triangle}$;MFCS4$^{\triangle/\triangle}$ mice, in which *Shh* expression was suppressed in Hedgehog-producing cells by removing the *Shh* enhancers, form supernumerary teeth (Sagai et al. 2017; Seo et al. 2018). The complete absence of epithelial *Shh* and *Smo* in *Krt14-cre;Shh*$^{flox/-}$and *Krt14-cre;Smo*$^{flox/flox}$ mice, respectively, leads to the molar fusion (Dassule et al. 2000; Gritli-Linde et al. 2002). Treatment with anti-Shh antibody or Hedgehog signaling inhibitors blocks the activity of Hedgehog signaling in Hedgehog-responsive cells, resulting in the supernumerary tooth formation and molar fusion (Cho et al. 2011; Mao et al. 2022). Molar fusion has been found also in mice deficient in *Evc, Evc2,* or *Ofd1* (Nakatomi et al. 2013; Liu et al. 2014; Zhang et al. 2022; Thivichon-

Prince et al. 2009). However, molar fusion was not found in *Cilk1*-deficient mice in the present study.

Supernumerary teeth can be obtained in the hybrid mice between different mutant mice that have a genetic defect in Hedgehog signaling but show normal tooth patterns. *Sostdc1*$^{+/-}$;*Shh*$^{+/-}$ mice, which were created by crossing *Sostdc1*$^{+/-}$ mice and *Shh*$^{+/-}$ mice with normal tooth pattern, showed supernumerary teeth (Ahn et al. 2010). However, there has been still no clear evidence as to whether molar fusion can be induced in hybrid mice between two different kinds of mutant mice with supernumerary teeth. In the present study, *Cilk1*$^{-/-}$;PCS1−MRCS1$^{\triangle/\triangle}$ mice created by crossing *Cilk1*$^{-/-}$ mice and PCS1−MRCS1$^{\triangle/\triangle}$ mice with supernumerary teeth showed fused molars in maxilla. The synergy observed in this hybrid mice is probably due to the simultaneous suppression of Hedgehog signaling in Hedgehog-producing cells and Hedgehog-responsive cells by PCS1−MRCS1 deletion and *Cilk1* deficiency, respectively (Fig. 13). This result strongly suggests that supernumerary teeth and molar fusion occur sequentially as Hedgehog signaling activity gradually declines. Unlike maxilla, the mandibles of *Cilk1*$^{-/-}$;PCS1−MRCS1$^{\triangle/\triangle}$ mice showed only supernumerary teeth, which was very similar to the previous results in *Evc* or *Evc2*-deficient mice. In *Evc* mutant mice, molar fusion occurs in maxilla and mandible at a penetrance of 100% and 17%, respectively (Nakatomi et al. 2013). *Evc2* deficiency leads to molar fusion in maxilla, but only the supernumerary tooth in mandible (Zhang et al. 2022). The cause of this difference in molar fusion susceptibility between maxilla and

mandible remains unclear.

Understanding tooth patterns in some mice with significantly decreased Hedgehog or Wnt signaling activity can be challenging. *Gas1*$^{+/-}$ mice and *Shh*$^{GFP/+}$ show normal molar development, and approximately 80% of *Gas1*$^{-/-}$ mice form supernumerary teeth. However, it has been reported that the penetration of supernumerary teeth is reduced to 38% in *Gas1*$^{-/-}$;*Shh*$^{GFP/+}$ mice (Seppala et al., 2022). *Wnt10b*$^{-/-}$ mice exhibit a regular tooth pattern, and 80% of *Wnt10a*$^{+/-}$;*Wnt10b*$^{-/-}$ mice have supernumerary teeth. However, *Wnt10a*$^{-/-}$;*Wnt10b*$^{-/-}$ mice, despite having the significantly small molars, and significantly reduced maxilla, mandible, and the body length, exhibit only three molars, with the first notably larger than the second, leading to the determination that supernumerary teeth are absent in these mice (Yoshinaga et al. 2023). Similar tooth patterns were observed in the present study. The R2/M1 ratio in *Cilk1*$^{-/-}$;PCS1−MRCS1$^{\triangle/\triangle}$ mice was about 1 on average, but was over 2 in some mice. Furthermore R2/M1 ratio was larger in *Cilk1*$^{-/-}$;PCS1−MRCS1$^{\triangle/\triangle}$ mice than in *Cilk1*$^{-/-}$ mice and PCS1−MRCS1$^{\triangle/\triangle}$ mice. These findings indicates that as Hedgehog signaling activity decreases, the size of the supernumerary tooth increases, possibly surpassing the M1 size. Likewise, in mice with genetically significantly reduced Hedgehog or Wnt signaling activity, such as *Gas1*$^{-/-}$;*Shh*$^{GFP/+}$ mice and *Wnt10a*$^{-/-}$;*Wnt10b*$^{-/-}$ mice, the most mesial tooth is likely to be supernumerary tooth. Additionally, it is suggested that the surpass of R2 over the size of M1 in these mutant mice resulted from a minor fusion between R2 and M1.

Tooth patterning is governed by the Wnt-Shh-Sostdc1 negative feedback loop (Cho et al. 2011), where a reduction in Hedgehog signaling activity leads to a decrease in the inhibitor Sostdc1. A hypothetic mechanism for tooth pattern formation determined by Hedgehog signaling during tooth development is proposed here. In wild-type mice, the R2 at E14 is degenerated by inhibitors produced by M1, resulting in the three-molar patterns. Conversely, in mice with reduced Hedgehog signaling activity, R2 persists instead of regressing due to decreased inhibitor levels following a reduction in mediators in M1. As Hedgehog signaling activity diminishes, the mutual interference effect between teeth decreases, allowing R2 to increase in size up to a certain threshold. With further downregulation of Hedgehog signaling, inhibitors are lost in both R2 and M1, leading to their fusion (Fig. 14).

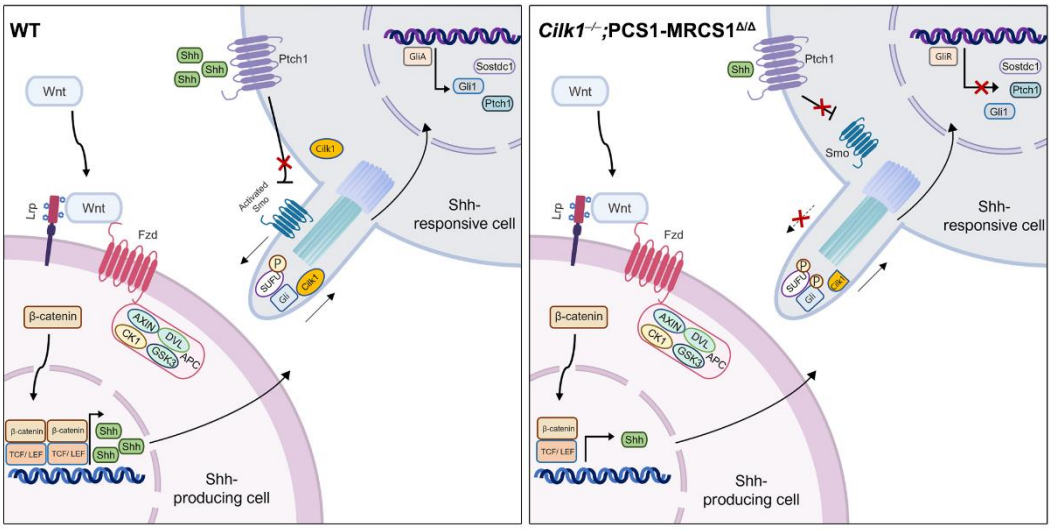

Figure 13. A scheme showing the interaction between Shh-producing and -responsive cells

In wild-type mice, Shh proteins are secreted due to increased Wnt signaling activity in Shh-producing cells. These proteins then bind to Ptch1 in Shh-responsive cells, activating Smo and allowing GliA to enter the nucleus to transcribe Hedgehog signaling target genes. However, in *Cilk1*$^{-/-}$;PCS1−MRCS1$^{\triangle/\triangle}$ mice, *Shh* transcription and Shh protein secretion are reduced. The absence of Cilk1 decreases Smo activation, leading to GliR instead of GliA entering the nucleus and preventing the transcription of target genes.

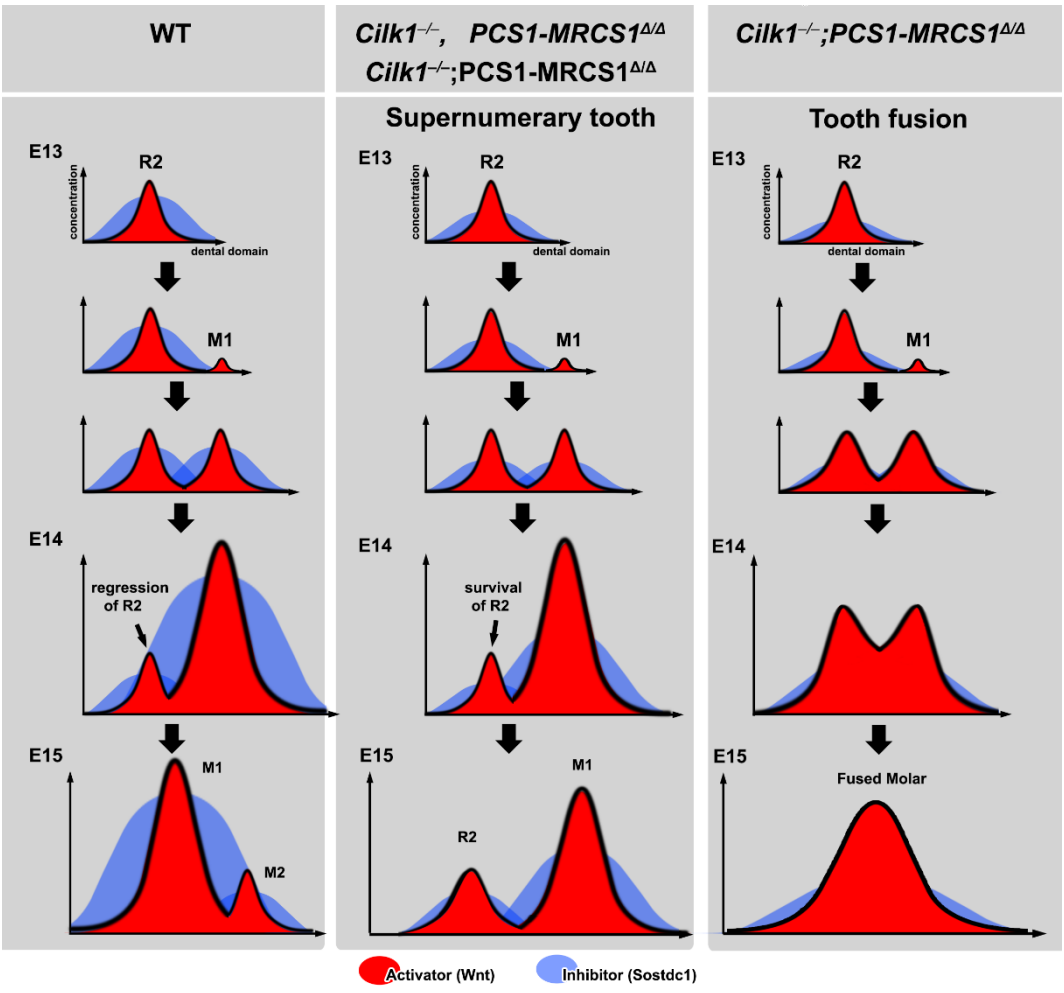

Figure 14. A hypothetical model for elucidating tooth pattern formation: exploring how R2 and M1 interact, influenced by Hedgehog signaling

V. CONCLUSION

Collectively, the findings of this study elucidate the pivotal role of Cilk1 in the formation and functionality of the primary cilia, which serves as a mediating organelle of Hedgehog signaling. By modulating Hedgehog signaling activity in both the producing and responsive cells, the study observed the occurrence of molar fusion alongside the emergence of supernumerary teeth with varying sizes. This diversity in tooth patterns contributes to a deeper understanding of the underlying mechanisms governing tooth pattern formation and facilitates the analysis of unusual tooth patterns.

VI. REFERENCES

Abigail S. Tucker, Karen L. Matthews, Paul T. Sharpe. 1998. '<Transformation of Tooth Type Induced by Inhibition of BMP Signaling.pdf>', *science*, 282: 1136-38.

Ahn, Y., B. W. Sanderson, O. D. Klein, and R. Krumlauf. 2010. 'Inhibition of Wnt signaling by Wise (Sostdc1) and negative feedback from Shh controls tooth number and patterning', *Development*, 137: 3221-31.

Anvarian, Z., K. Mykytyn, S. Mukhopadhyay, L. B. Pedersen, and S. T. Christensen. 2019. 'Cellular signalling by primary cilia in development, organ function and disease', *Nature Reviews Nephrology*, 15: 199-219.

Baujat, Geneviève, and Martine Le Merrer. 2007. 'Ellis-van Creveld syndrome', *Orphanet journal of rare diseases*, 2: 1-5.

Brugmann, S. A., N. C. Allen, A. W. James, Z. Mekonnen, E. Madan, and J. A. Helms. 2010. 'A primary cilia-dependent etiology for midline facial disorders', *Human Molecular Genetics*, 19: 1577-92.

Bureau, A., M. M. Parker, I. Ruczinski, M. A. Taub, M. L. Marazita, J. C. Murray, E. Mangold, M. M. Noethen, K. U. Ludwig, J. B. Hetmanski, J. E. Bailey-Wilson, C. D. Cropp, Q. Li, S. Szymczak, H. Albacha-Hejazi, K. Alqosayer, L. L. Field, Y. H. Wu-Chou, K. F. Doheny, H. Ling, A. F. Scott, and T. H. Beaty. 2014. 'Whole Exome Sequencing of Distant Relatives in Multiplex Families Implicates Rare Variants in Candidate Genes for Oral Clefts', *Genetics*, 197: 1039-+.

Chaya, Taro, Yoshihiro Omori, Ryusuke Kuwahara, and Takahisa Furukawa. 2014. 'ICK is essential for cell type‐specific ciliogenesis and the regulation of ciliary transport', *The EMBO Journal*, 33: 1227-42.

Cho, S. W., S. Kwak, T. E. Woolley, M. J. Lee, E. J. Kim, R. E. Baker, H. J. Kim, J. S. Shin, C. Tickle, P. K. Maini, and H. S. Jung. 2011. 'Interactions between Shh, Sostdc1 and Wnt signaling and a new feedback loop for spatial patterning of the teeth', *Development*, 138: 1807-16.

Christensen, S. T., L. B. Pedersen, L. Schneider, and P. Satir. 2007. 'Sensory cilia and integration of signal transduction in human health and disease', *Traffic*, 8: 97-109.

Curry, CJ, and BD Hall. 1979. 'Polydactyly, conical teeth, nail dysplasia, and short limbs: a new autosomal dominant malformation syndrome', *Birth Defects Original Article Series*, 15: 253-63.

Dassule, H. R., P. Lewis, M. Bei, R. Maas, and A. P. McMahon. 2000. 'Sonic hedgehog regulates growth and morphogenesis of the tooth', *Development*, 127: 4775-85.

Dodge, JA, and DC Kernohan. 1967. 'Oral-facial-digital syndrome', *Archives of disease in childhood*, 42: 214.

Dorn, K. V., C. E. Hughes, and R. Rohatgi. 2012. 'A Smoothened-Evc2 Complex Transduces the Hedgehog Signal at Primary Cilia', *Developmental Cell*, 23: 823-35.

Durandau, E., and S. Pelet. 2021. 'Cross-regulation between CDK and MAPK control cellular fate', *Quantitative Biology*, 9: 341-59.

Fedorov, A., R. Beichel, J. Kalpathy-Cramer, J. Finet, J. C. Fillion-Robin, S. Pujol, C. Bauer, D. Jennings, F. Fennessy, M. Sonka, J. Buatti, S. Aylward, J. V. Miller, S. Pieper, and R. Kikinis. 2012. '3D Slicer as an image computing platform for the Quantitative Imaging Network', *Magn Reson Imaging*, 30: 1323-41.

Ferrante, M. I., A. Zullo, A. Barra, S. Bimonte, N. Messaddeq, M. Studer, P. Dollé, and B. Franco. 2006. 'Oral-facial-digital type I protein is required for primary cilia formation and left-right axis specification', *Nature Genetics*, 38: 112-17.

Fu, Zheng, Casey D Gailey, Eric J Wang, and David L Brautigan. 2019. 'Ciliogenesis associated kinase 1: targets and functions in various organ systems', *FEBS letters*, 593: 2990-3002.

García-García, M. J., J. T. Eggenschwiler, T. Caspary, H. L. Alcorn, M. R. Wyler, D. Huangfu, A. S. Rakeman, J. D. Lee, E. H. Feinberg, J. R. Timmer, and K. V. Anderson. 2005. 'Analysis of mouse embryonic patterning and morphogenesis by forward genetics', *Proceedings of the National Academy of Sciences of the United States of America*, 102: 5913-19.

Goetz, S. C., and K. V. Anderson. 2010. 'The primary cilium: a signalling centre during vertebrate development', *Nat Rev Genet*, 11: 331-44.

Gritli-Linde, A., M. Bei, R. Maas, X. Y. M. Zhang, A. Linde, and A. P. McMahon. 2002. 'Shh signaling within the dental epithelium is necessary for cell proliferation, growth and polarization', *Development*, 129: 5323-37.

Hampl, M., P. Cela, H. L. Szabo-Rogers, M. Kunova Bosakova, H. Dosedelova, P. Krejci, and M. Buchtova. 2017. 'Role of Primary Cilia in Odontogenesis', *J Dent Res*, 96: 965-74.

Hisamoto, M., M. Goto, M. Muto, J. Nio-Kobayashi, T. Iwanaga, and A. Yokoyama. 2016. 'Developmental changes in primary cilia in the mouse tooth germ and oral cavity', *Biomedical Research-Tokyo*, 37: 207-14.

Huangfu, D. W., A. M. Liu, A. S. Rakeman, N. S. Murcia, L. Niswander, and K. V. Anderson. 2003. 'Hedgehog signalling in the mouse requires intraflagellar transport proteins', *Nature*, 426: 83-87.

Jing, J., J. Feng, Y. Yuan, T. Guo, J. Lei, F. Pei, T. V. Ho, and Y. Chai. 2022. 'Spatiotemporal

single-cell regulatory atlas reveals neural crest lineage diversification and cellular function during tooth morphogenesis', *Nat Commun*, 13: 4803.

Kanady, J. D., S. J. Munger, M. H. Witte, and A. M. Simon. 2015. 'Combining Foxc2 and Connexin37 deletions in mice leads to severe defects in lymphatic vascular growth and remodeling', *Dev Biol*, 405: 33-46.

Kudo, T., M. Kawasaki, K. Kawasaki, F. Meguro, J. Nihara, I. Honda, M. Kitamura, A. Fujita, K. Osawa, K. Ichikawa, T. Nagai, Y. Ishida, P. T. Sharpe, T. Maeda, I. Saito, and A. Ohazama. 2023. 'Ift88 regulates enamel formation via involving Shh signaling', *Oral Diseases*, 29: 1622-31.

Lahiry, P., J. Wang, J. F. Robinson, J. P. Turowec, D. W. Litchfield, M. B. Lanktree, G. B. Gloor, E. G. Puffenberger, K. A. Strauss, M. B. Martens, D. A. Ramsay, C. A. Rupar, V. Siu, and R. A. Hegele. 2009. 'A Multiplex Human Syndrome Implicates a Key Role for Intestinal Cell Kinase in Development of Central Nervous, Skeletal, and Endocrine Systems (vol 84, pg 134, 2009)', *American Journal of Human Genetics*, 84: 822-22.

Lee, K. H. 2020. 'Involvement of Wnt signaling in primary cilia assembly and disassembly', *FEBS J*, 287: 5027-38.

Levin, L Stefan, JC Perrin, Leiv Ose, John P Dorst, J Daniel Miller, and Victor A McKusick. 1977. 'A heritable syndrome of craniosynostosis, short thin hair, dental abnormalities, and short limbs: cranioectodermal dysplasia', *The Journal of Pediatrics*, 90: 55-61.

Lew, J. 2003. 'MAP kinases and CDKs: Kinetic basis for catalytic activation', *Biochemistry*, 42: 849-56.

Li, G., M. Liu, S. Zhang, H. Wan, Q. Zhang, R. Yue, X. Yan, X. Wang, Z. Wang, and Y. Sun. 2018. 'Essential Role of IFT140 in Promoting Dentinogenesis', *Journal of Dental Research*, 97: 423-31.

Liu, B., S. Chen, D. Cheng, W. Jing, and J. A. Helms. 2014. 'Primary Cilia Integrate Hedgehog and Wnt Signaling during Tooth Development', *Journal of Dental Research*, 93: 475-82.

Manning, G., D. B. Whyte, R. Martinez, T. Hunter, and S. Sudarsanam. 2002. 'The protein kinase complement of the human genome', *science*, 298: 1912-+.

Mao, C. Q., Y. Z. Lai, C. Y. Liao, J. P. Chen, Y. H. Hong, C. Y. Ren, C. Y. Wang, M. Lu, and W. H. Chen. 2022. 'Revitalizing mouse diphyodontic dentition formation by inhibiting the sonic hedgehog signaling pathway', *Developmental Dynamics*, 251: 759-76.

Mill, P., S. T. Christensen, and L. B. Pedersen. 2023. 'Primary cilia as dynamic and diverse signalling hubs in development and disease', *Nat Rev Genet*, 24: 421-41.

Moon, H., J. Song, J. O. Shin, H. Lee, H. K. Kim, J. T. Eggenschwiller, J. Bok, and H. W. Ko. 2014. 'Intestinal cell kinase, a protein associated with endocrine-cerebro-osteodysplasia syndrome, is a key regulator of cilia length and Hedgehog signaling', *Proc Natl Acad Sci U S A*, 111: 8541-6.

Nakamura, Kentaro, Tatsuro Noguchi, Mariko Takahara, Yoshihiro Omori, Takahisa Furukawa, Yohei Katoh, and Kazuhisa Nakayama. 2020. 'Anterograde trafficking of ciliary MAP kinase–like ICK/CILK1 by the intraflagellar transport machinery is required for intraciliary retrograde protein trafficking', *Journal of Biological Chemistry*, 295: 13363-76.

Nakatomi, M., M. Hovorakova, A. Gritli-Linde, H. J. Blair, K. MacArthur, M. Peterka, H. Lesot, R. Peterkova, V. L. Ruiz-Perez, J. A. Goodship, and H. Peters. 2013. 'Evc regulates a symmetrical response to Shh signaling in molar development', *J Dent Res*, 92: 222-8.

Ohazama, A., C. J. Haycraft, M. Seppala, J. Blackburn, S. Ghafoor, M. Cobourne, D. C. Martinelli, C. M. Fan, R. Peterkova, H. Lesot, B. K. Yoder, and P. T. Sharpe. 2009. 'Primary cilia regulate Shh activity in the control of molar tooth number', *Development*, 136: 897-903.

Oud, Machteld M, Carine Bonnard, Dorus A Mans, Umut Altunoglu, Sumanty Tohari, Alvin Yu Jin Ng, Ascia Eskin, Hane Lee, C Anthony Rupar, and Nathalie P de Wagenaar. 2016. 'A novel ICK mutation causes ciliary disruption and lethal endocrine-cerebro-osteodysplasia syndrome', *Cilia*, 5: 1-11.

Reiter, J. F., and M. R. Leroux. 2017. 'Genes and molecular pathways underpinning ciliopathies', *Nature Reviews Molecular Cell Biology*, 18: 533-47.

Sagai, T., T. Amano, A. Maeno, H. Kiyonari, H. Seo, S. W. Cho, and T. Shiroishi. 2017. 'SHH signaling directed by two oral epithelium-specific enhancers controls tooth and oral development', *Scientific Reports*, 7.

Salazar-Ciudad, I. 2012. 'Tooth patterning and evolution', *Curr Opin Genet Dev*, 22: 585-92.

Satoda, Y., T. Noguchi, T. Fujii, A. Taniguchi, Y. Katoh, and K. Nakayama. 2022a. 'BROMI/TBC1D32 together with CCRK/CDK20 and FAM149B1/JBTS36 contributes to intraflagellar transport turnaround involving ICK/CILK1', *Mol Biol Cell*, 33: ar79.

Satoda, Yuuki, Tatsuro Noguchi, Taiju Fujii, Aoi Taniguchi, Yohei Katoh, and Kazuhisa Nakayama. 2022b. 'BROMI/TBC1D32 together with CCRK/CDK20 and FAM149B1/JBTS36 contributes to intraflagellar transport turnaround involving ICK/CILK1', *Molecular biology of the cell*, 33: ar79.

Seo, H., T. Amano, R. Seki, T. Sagai, J. Kim, S. W. Cho, and T. Shiroishi. 2018. 'Upstream

Enhancer Elements of Shh Regulate Oral and Dental Patterning', *J Dent Res*, 97: 1055-63.

Shin, J. O., J. Song, H. S. Choi, J. Lee, K. Lee, H. W. Ko, and J. Bok. 2019. 'Activation of sonic hedgehog signaling by a Smoothened agonist restores congenital defects in mouse models of endocrine-cerebro-osteodysplasia syndrome', *EBioMedicine*, 49: 305-17.

Susami, Takafumi, Takayuki Kuroda, Hidemi Yoshimasu, and Ruri Suzuki. 1999. 'Ellis-van Creveld syndrome: craniofacial morphology and multidisciplinary treatment', *The Cleft palate-craniofacial journal*, 36: 345-52.

Thesleff, I. 1995. 'Tooth morphogenesis', *Adv Dent Res*, 9: 12.

Thesleff, I. 2003. 'Epithelial-mesenchymal signalling regulating tooth morphogenesis', *J Cell Sci*, 116: 1647-8.

Thivichon-Prince, B., M. L. Couble, A. Giamarchi, P. Delmas, B. Franco, L. Romio, T. Struys, I. Lambrichts, D. Ressnikoff, H. Magloire, and F. Bleicher. 2009. 'Primary cilia of odontoblasts: possible role in molar morphogenesis', *J Dent Res*, 88: 910-5.

Tian, H., J. F. Feng, J. Y. Li, T. V. Ho, Y. Yuan, Y. Liu, F. Brindopke, J. C. Figueiredo, W. Magee, P. A. Sanchez-Lara, and Y. Chai. 2017. 'Intraflagellar transport 88 (IFT88) is crucial for craniofacial development in mice and is a candidate gene for human cleft lip and palate', *Human Molecular Genetics*, 26: 860-72.

Walczak-Sztulpa, J., J. Eggenschwiler, D. Osborn, D. A. Brown, F. Emma, C. Klingenberg, R. C. Hennekam, G. Torre, M. Garshasbi, A. Tzschach, M. Szczepanska, M. Krawczynski, J. Zachwieja, D. Zwolinska, P. L. Beales, H. H. Ropers, A. Latos-Bielenska, and A. W. Kuss. 2010. 'Cranioectodermal Dysplasia, Sensenbrenner Syndrome, Is a Ciliopathy Caused by Mutations in the Gene', *American Journal of Human Genetics*, 86: 949-56.

Wheway, G., L. Nazlamova, and J. T. Hancock. 2018. 'Signaling through the Primary Cilium', *Front Cell Dev Biol*, 6: 8.

Willaredt, M. A., K. Hasenpusch-Theil, H. A. R. Gardner, I. Kitanovic, V. C. Hirschfeld-Warneken, C. P. Gojak, K. Gorgas, C. L. Bradford, J. Spatz, S. Wölfl, T. Theil, and K. L. Tucker. 2008. 'A Crucial Role for Primary Cilia in Cortical Morphogenesis', *Journal of Neuroscience*, 28: 12887-900.

Yanardag, S., and E. N. Pugacheva. 2021. 'Primary Cilium Is Involved in Stem Cell Differentiation and Renewal through the Regulation of Multiple Signaling Pathways', *Cells*, 10.

Yang, Y., P. Paivinen, C. Xie, A. L. Krup, T. P. Makela, K. E. Mostov, and J. F. Reiter. 2021. 'Ciliary Hedgehog signaling patterns the digestive system to generate mechanical

forces driving elongation', *Nat Commun*, 12: 7186.

Yang, Y., N. Roine, and T. P. Makela. 2013. 'CCRK depletion inhibits glioblastoma cell proliferation in a cilium-dependent manner', *EMBO Rep*, 14: 741-7.

Yoshinaga, K., A. Yasue, S. N. Mitsui, Y. Minegishi, S. Oyadomari, I. Imoto, and E. Tanaka. 2023. 'Effects of Wnt10a and Wnt10b Double Mutations on Tooth Development', *Genes*, 14.

Yuan, G. J., G. Singh, S. Chen, K. C. Perez, Y. Wu, B. Liu, and J. A. Helms. 2017. 'Cleft Palate and Aglossia Result From Perturbations in Wnt and Hedgehog Signaling', *Cleft Palate-Craniofacial Journal*, 54: 269-80.

Yuan, X., X. Cao, and S. Y. Yang. 2019. 'IFT80 is required for stem cell proliferation, differentiation, and odontoblast polarization during tooth development', *Cell Death & Disease*, 10.

Zhang, H. H., A. Chinoy, P. Mousavi, A. Beeler, K. Louie, C. Collier, and Y. Mishina. 2022. 'Elevated WNT signaling and compromised Hedgehog signaling due to Evc2 loss of function contribute to the abnormal molar patterning', *Frontiers in Dental Medicine*, 3.

Zhang, Z. C., B. J. Wlodarczyk, K. Niederreither, S. Venugopalan, S. Florez, R. H. Finnell, and B. A. Amendt. 2011. 'FUZ Regulates Craniofacial Development through Tissue Specific Responses to Signaling Factors', *Plos One*, 6.

ABSTRACT (IN KOREAN)

치아패턴 형성 과정 중
Hedgehog pathway 조절을 통한 Cilk1 유전자의 역할

경민재
(지도교수: 조성원)
연세대학교 대학원
응용생명과학과

일차섬모(primary cilia)는 척추동물에서 외부의 신호를 세포 내부로 전달하는 세포소기관으로서 발생과 조직 항상성 유지에 필수적이다. *Cilk1* (Ciliogenesis associated kinase 1) 유전자는 일차섬모에서 섬모 형성 및 기능에 중요한 역할을 하는 유전자이다. *Cilk1*의 기능이 상실되면 Hedgehog 신호 전달경로에 문제가 발생한다고 보고되었고, *Cilk1*−결핍 마우스에서 다지증, 감각계 기능 이상, 구개열과 같은 심각한 섬모병증(Ciliopathy)이 발생한다고 알려져 있다. 그러나 치아 형성에서 *Cilk1*의 역할은 아직 보고된 바 없다.

본 연구에서는 정상 마우스의 치배(tooth germ)에서 *Cilk1* 유전자의 발현 위치를 확인하였고, *Cilk1*−결핍 마우스에서 일차섬모의 길이 변화와 치아패턴의 변화를 확인하였다. 실험 결과, *Cilk1*은 치배의 거의 모든 세포에서 발현되었다. *Cilk1*−결

핍 마우스의 치배에서 일차섬모의 길이가 증가하고, Hedgehog 신호 전달경로의 활성이 감소되면서, *Cilk1*-결핍 마우스의 상악과 하악 모두에서 과잉치가 형성되었음을 확인하였다. 추가로, 과잉치를 보이는 Shh 인핸서 결손 마우스인 PCS1-MRCS1$^{\triangle/\triangle}$ 마우스와 *Cilk1*-결핍 마우스의 교차 교배를 통해 제작된 *Cilk1*$^{-/-}$;PCS1-MRCS1$^{\triangle/\triangle}$ 마우스는 상악에서 치아융합을 보였고, 하악에서는 과잉치의 크기 증가를 나타냈다. 이러한 결과를 통해, *Cilk1*이 치배에서도 Hedgehog 신호전달경로를 조절한다는 것을 확인하였고, Hedgehog 신호전달경로의 활성 정도에 따라 치아패턴이 세밀하게 조절된다는 것을 확인하였다.

중심단어 : 섬모형성 관련 인산화효소-1 (Cilk1), SHH 신호전달, 치아 발생, 과잉치, 일차섬모